Aalborg University
Department of Energy Technology

Hierarchical Control of an AC Microgrid

Author:
Group PED3 - 941
Roberto Airi

Supervisors:
Josep M. Guerrero
Juan C. Vasquez

June 1, 2018

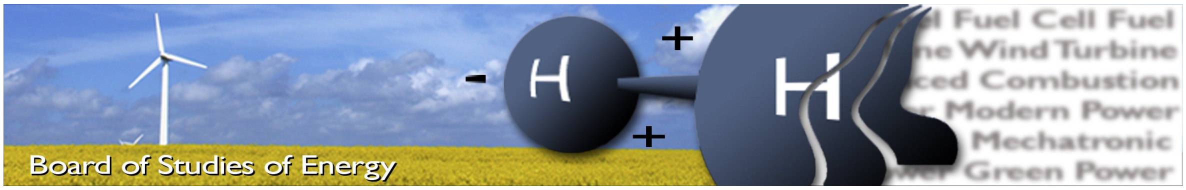

Title:	Hierarchical Control of an AC Microgrid
Semester:	MSc. 3^{rd} and 4^{th} Semester
Semester theme:	Master Thesis
Project period:	01.09.17 to 01.06.18
ECTS:	50
Supervisor:	Josep M. Guerrero, Juan C. Vasquez
Project group:	PED3-941

SYNOPSIS:

As well known the grid is facing a big change due to the spreading of the Renewable Energy Sources (RES). The increasing deployment of Distribute Energy Resources (DER) poses several difficulties to the Transmission System Operators (TSOs). Among them there are the grid-connection, the constant power production, the protections and in general grid standards fulfillment. These issues are related to the bidirectional power flow in the grid and to the stochastic behavior of the primary source of energy, e.g. sun and wind.
Dealing with the aforementioned problems, with respect to the microsources ($< 100kW$), the MicroGrids (MGs) deployment seems to be one of the most effective solutions. Indeed, the final user becomes an active part of the grid or "prosumer". Through the employment of power electronics interfaces for prime movers, the prosumer is able e.g. to enhance the local reliability of the distribution network and to reduce the feeder's losses, meeting the power quality requirements.
Among the several strategies in the literature, the hierarchical control is an attractive one due to its flexibility and reliability. For these reasons, in this thesis the hierarchical control has been studied and implemented on an AC Microgrid.

Roberto Airi

Pages, total: 50
Appendix: 2

By accepting the request from the fellow student who uploads the study group's project report in Digital Exam System, you confirm that all group members have participated in the project work, and thereby all members are collectively liable for the contents of the report. Furthermore, all group members confirm that the report does not include plagiarism.

Symbols Specification

Symbol	**Specification**	**Unit**
S	Apparent power	VA
Q	Reactive power	Var
P	Active power	W
V	Voltage	V
I	Current	A
Z	Impedance	Ω
L	Inductance	H
R	Resistance	Ω
C	Capacitance	F
$\cos\phi$	Power factor	-
d	Duty Cycle	-
f	Frequency	Hz
T	Period	s
ω	Angular frequency	rad/s

Acronyms

Acronym	**Specification**
CCM	Current Controlled Mode
DER	Distributed Energy Resources
DG	Distributed Generator
DNO	Distribution Network Operator
DSP	Digital Signal Processor
EMS	Energy Management System
ESS	Energy Storage System
FPGA	Field Programmable Gate Array
MG	MicroGrid
MPPT	Maximum Power Point Tracking
PCC	Point of Common Coupling
PI	Proportional Integral
PID	Proportional Integral Derivative
PLL	Phase-Locked Loop
PR	Proportional Resonant
PWM	Pulse Width Modulation
PV	Photovoltaic
RES	Renewable Energy System
RMS	Root Mean Squared
SG	Synchronous Generator
STS	Static Transfer Switch
THD	Total Harmonic Distortion
TSO	Transmission System Operator
VCM	Voltage Controlled Mode
VSI	Voltage Source Inverter

Contents

Preface

This thesis report summarizes the work that has been carried out during the 9th and 10th semesters of the Master of Science in Power Electronics and Drives. The control of an AC Microgrid has been chosen by the author as a long-thesis project in Fall 2017.

The project deals with the hierarchical control of an AC Microgrid, an attractive topic for what regards the development of the medium and low voltage grid. Given the topic, the work on the project has been relevant in the education of the author. In fact, it gave to the author the possibility to work on a hot topic in the research environment. Moreover, the thesis let the author strengthen his knowledge in:

- Background of Microgrids;
- Design of a controller with different approaches;
- Interaction between different control levels;
- Control of a complex system with nested loops;
- Issues related to the parallel connection of Voltage Source Inverters (VSIs).

In conclusion, the author would like to give a special thanks to Dr. Yajuan Guan and to the supervisors Prof. Josep M. Guerrero and Assoc. Prof. Juan C. Vasquez for their guidance, availability and support during all the project.

INTRODUCTION

Chapter 1

Introduction

In this chapter a brief description of the reasons of the transition to distributed renewable sources is given at first. Afterwards, the issues related to the increase of energy demand and to a high penetration of renewable energy sources are analyzed. A possible solution to these problems has been found in the Microgrid concept, which is briefly described, mentioning also the ongoing projects around the World. The chapter ends with the thesis objectives and thesis outline.

1.1 Background and Motivations

In the last decades, humanity witnessed a technological development at rates never experienced before. Among the consequences, can be numbered an unexpected increase of the energy demand over the years and the reduction of fossil fuels due to their massive deployment and finite availability [1]. The former is becoming an unbearable burden on the transmission network, while the latter, together with the awareness of the harmful effects of fossil fuels burning both on humans and environment [2, 3], has brought to the spreading of renewable energy sources.

Investigating the effects of the aforementioned consequences, the growth of installed RES introduces new problems in the grid due to the stochastic behavior of their prime mover e.g. sun and wind [4]. Indeed, it is more difficult to deliver constant power following the loads demand when the power production is not constant. For this reason and due to the increase of efficiency and reliability and the decrease of cost of power electronics, converters have been largely deployed [5]. Moreover, using the proper control strategies is possible also to improve the power quality e.g. doing voltage harmonics compensation [6].

For what concerns the burden on the main grid, since the improvement of the transmission network is economically challenging, a cost effective solution has been found in MicroGrids or MiniGrids [7]. In fact, as the name suggests, the MG works like a small scale grid and is able to provide both electricity and heat to the loads. Moreover, it lets the power produced by the DG units flows directly to the loads without having to pass trough the transmission network, avoiding more losses. In Fig.1.1 the general structure of a MicroGrid is depicted. As aformentioned, the MG is able to deliver not only electricity but also heat, therefore along with RES also microturbines, fuel cells, diesel generators etc. can be found. Nevertheless, to provide constant power to the loads in spite of the stochastic behavior of the RES, also Energy Storage Systems (ESSs) are embedded in the system [8].

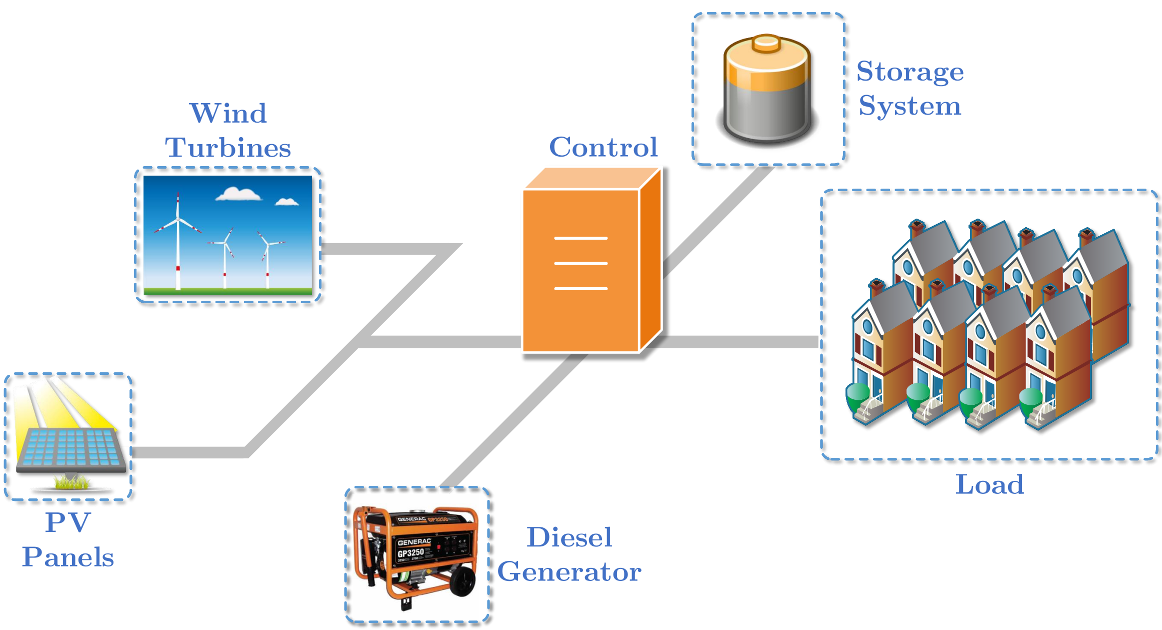

Fig. 1.1: Conceptual scheme of a MicroGrid.

The energy sources are connected to a common bus by mean of converters so that the power can flow either to the loads and to the storage systems when needed or to the grid when the produced power exceeds the needs of the MG. In fact, the MicroGrid is able to operate in two modes: connected to the grid and disconnected from the grid. They are commonly referred as grid-connected mode and islanded mode respectively. When connected to the grid, the MG acts as a load/source and its main duty is the control of the output power, since the voltage at the Point of Common Coupling (PCC) and the frequency references together with the balance between produced and demanded power are managed by the main grid. When the MG is in islanded mode, its control is more complex because it has to perform voltage and frequency control and has to take care about the balance between supply and demand, the power quality and the communication between the several components of the MG [9]. To pass from one state to the other, a Static Transfer Switch(STS) is used. It is a smart switch able to recognize, after the evaluation of grid's and MG's status based on feedback measurements, whether the MicroGrid should be connected or not to the transmission network [10].

As can be inferred from the previous analysis, the integration of DGs and ESSs with the MGs not only ensures to lighten the burden on the main grid but also allows to cope with the penetration of RES. This cooperation is particularly advantageous since it provides higher reliability and flexibility to the grid. For instance, the possibility of intentional islanding is useful when e.g. there is a fault in the grid, since the MG can still operate thanks to the presence of several DGs and ESSs [8] so that the loads are always supplied. Looking further ahead, a massive diffusion of MicroGrids would be beneficial with respect to the concept of a smarter, more efficient, reliable and technologically advanced grid, known as Smart Grid (SG) [11].

On the other side, due to the bidirectional power flow introduced by the use of DGs, different protections are needed, since the previous ones installed were conceived for a unidirectional one: from the big power plants through the transmission and distribution lines to the loads. Moreover, while in big power plants the initial energy needed by new loads is provided using the energy stored in the generators inertia, in the micro sources, since they are inertia less, the introduction of new loads leads to power unbalances between generation and loads that needs to take care about [9]. Finally, also regulatory issues related to the grid connection of DGs need to be faced [12].

In Table 1.1 the SG characteristics are compared with the conventional power grid, giving a deeper understanding of the benefits of the transition to a smarter grid [13].

Conventional Grid	Smart Grid
Electromechanical	Digital
One-way communication	Two-way communication
Centralized generation	Distributed generation
Few sensors	Sensors throughout
Manual monitoring	Self-monitoring
Manual restoration	Self-healing
Failures and blackouts	Adaptive and islanding
Limited control	Pervasive control
Few customer choices	Many customer choices

Tab. 1.1: Comparison between the conventional power grid and the smart grid [13].

Going further, depending on the type of the common bus it is possible to have DC, AC or hybrid Microgrids, as shown in Fig.1.2 [14].

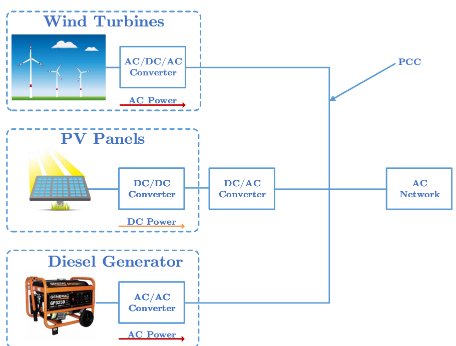

(a) Scheme of an AC MicroGrid.

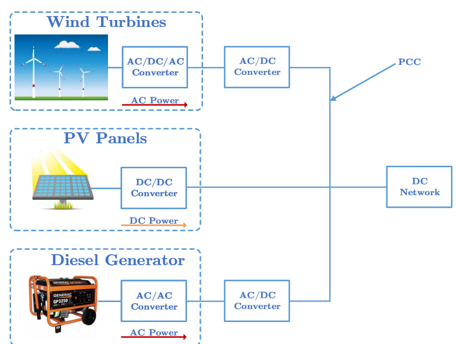

(b) Scheme of an DC MicroGrid.

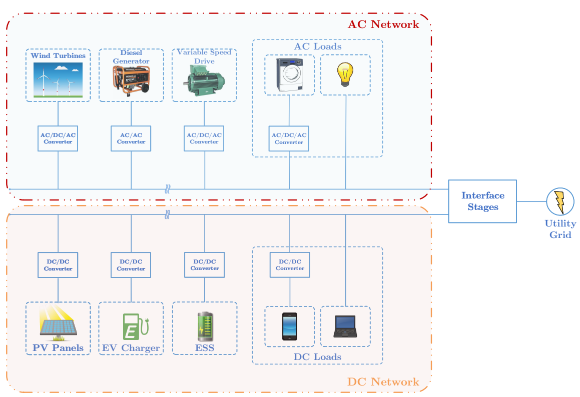

(c) Scheme of an Hybrid MicroGrid.

Fig. 1.2: Types of MG.

Hereafter a thorough analysis of the peculiarities and of the feasibility of each type of MicroGrid is carried out. The AC MicroGrid gives the opportunity to integrate DGs to the grid in a straightforward way avoiding significant modifications. Furthermore, due to the widespread range of protections on the market is possible to achieve an high fault management capability. Moreover, voltage levels can be easily modified using low frequency transformers. Nonetheless, the AC architecture presents some downsides like the need of synchronization by the DGs and the reactive power circulation that causes losses in the network grid. Moving to the DC MicroGrid, it is more efficient with respect to the AC one as less converters are needed and, because there is no reactive power production, no reactive current is circulating in the grid. Additionally, for the connection of DGs no synchronization process is needed. Anyway, the adaption of the distribution grid to the DC system implies consistent investments. Finally, for what regards the Hybrid MG, it combines the advantages of both AC and DC MGs, having a network for each MG type ensuring the direct integration of DGs, ESSs and loads to the AC or DC network respectively. At the same time, the protection aspect for the DC MG network is a problem, as mentioned before. Furthermore, also the management of such a structure is more complex due to the control needs of the devices connected to the AC and DC networks and also the control of the interface power converter [15].

Due to the ease of integration within the existing transmission network, in this project the focus is on the AC MicroGrids, whose pros and cons are briefly summarized in Table 1.2.

Pros	**Cons**
Lightens grid burden	Need lots of sensors
RES management	Need of more protections
Efficiency	Control complexity
Flexibility	Inertia-less
Fault ride-through capability	Circulating currents
Hot-swap operation capability	Lack of regulations

Tab. 1.2: Pros and Cons of Microgrids deployment.

1.2 Thesis Objectives

The evolution towards the smart grid passes through the use of modern technology for what regards converters, energy sources, protections and all the other grid components, communication technology and bidirectional power flow management. The result is a more flexible, reliable and efficient grid. In this scenario, the MG is its fundamental block and a cornerstone. Among the existing control strategies for a MicroGrid, the hierarchical control seems to be a good solution especially when it comes to standardization. It divides the control structure into three layers, namely primary, secondary and tertiary. One of the main duties of the primary level is the power sharing between the different converters. In its standard form, the secondary takes care about the voltage and frequency restoration caused by deviation on the primary level. The tertiary is the highest level and performs the energy management based on grid requests. In this project has been considered a likely scenario as the one in Fig.1.3, where the prime mover are PV panels and batteries are used in order to be able to storage the surplus power produced and supply the loads continuously. Furthermore, the system is able to switch from islanded- to grid-connected mode seamlessly. From now on, due to time limits, the DC-link voltage is considered constant and the main focus is on the control of the VSIs and their interactions with the grid and the loads.

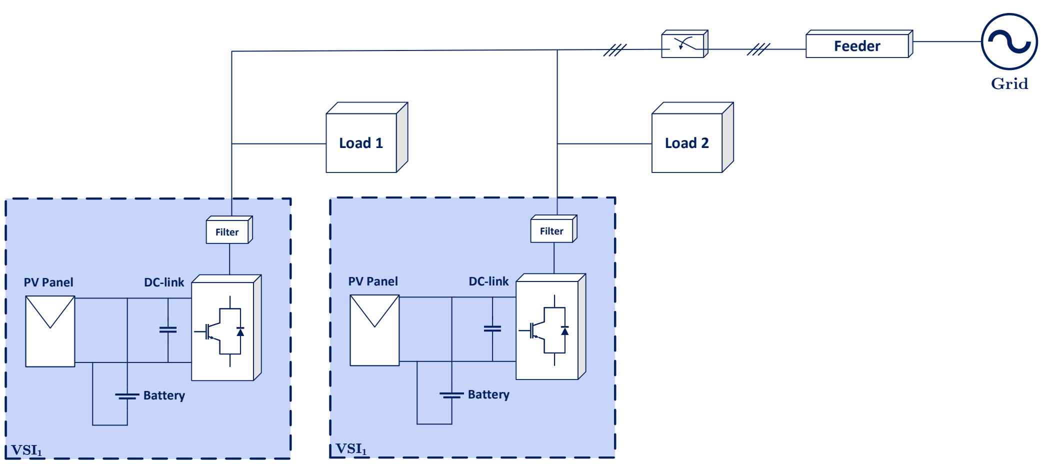

Fig. 1.3: Case scenario considered in this thesis work with two paralleled VSIs, where the DC-link can be considered constant thanks to a good design of the ESS and the PV panels.

This thesis claims to give a deeper understanding of the MicroGrid concept, particularly:

- Describe the hierarchical control strategy mentioning the most promising research trends;
- Develop the basic primary control, showing its strengths and weaknesses and implement some possible solutions i.e. the virtual impedance;
- Develop the secondary control, taking care of voltage and frequency restoration;
- Develop the Energy Management System (EMS) known also as tertiary control;
- Implementation of the whole control structure firstly through the use of the Hardware-in-the-Loop strategy, followed by the implementation on the actual setup;
- Validation of the control strategy adopted.

1.3 Outline of the Thesis

This thesis consists of two parts, six chapters and has one appendix. The aim of the first part is to describe the background and the The current chapter has described the status of the actual grid after the increase of energy demand and changes like the introduction of DGs and in particular more and more RESs, identifying in MicroGrids a convincing, cost effective solution.

In chapter two the MicroGrids' structure is firstly presented. Then, the duties of the MG in different operation modes, namely grid-connected and islanded, are described. Finally, a brief description of the existing control strategies is given, explaining why the hierarchical control seems to be one of the most promising. This is the end of the first part.

In the second part the hierarchical control is described in details. The third chapter is about the Primary control. Firstly the description of the nested loop approach regarding the voltage and current loops is carried out. After that, the reasons behind the choice of the droop control are stated, together with its drawbacks. The Chapter ends with the description of the synchronization loop.

The fourth chapter is dedicated to the Secondary Control. Here the frequency and the voltage restoration are described. They are needed as the droop control is employed. Furthermore, two approaches are described: the central secondary control and the distributed secondary control.

The analysis of the implemented MicroGrid control is the main focus of chapter six.

The last chapter presents conclusions regarding the results of simulation work and the future work that can be done.

Chapter 2

The Microgrid Concept: Operation and Control Architectures

2.1 Introduction

This chapter intends to give the basics of an AC Microgrid from different points of view. Starting from the description of its physical structure, continuing with an analysis of the peculiarities and the issues related to the Microgrid's operation modes, namely islanded and grid-connected. The first part of the report ends with a brief overview on the most known MG control strategies, motivating why among them the hierarchical control seems to be the most promising one.

2.2 Structure of a Microgrid

Despite the complexity of a Microgrid, it is possible to identify its fundamental elements which are the prime movers, the ESSs, the control unit and the loads. As an example, resuming Fig.1.1, the aforementioned elements are highlighted, resulting in Fig.2.1.

Starting from the prime movers, they are the energy sources and their type depends on the geographical configuration and raw material availability. The first affects the RES that can be used, i.e. wind turbine, PV panels, tidal or wave power and so on; the latter determines the type of non renewable energy employable, like diesel generators, fuel cells, microturbines etc.

From the the energy efficiency and the integration of RESs point of view, the

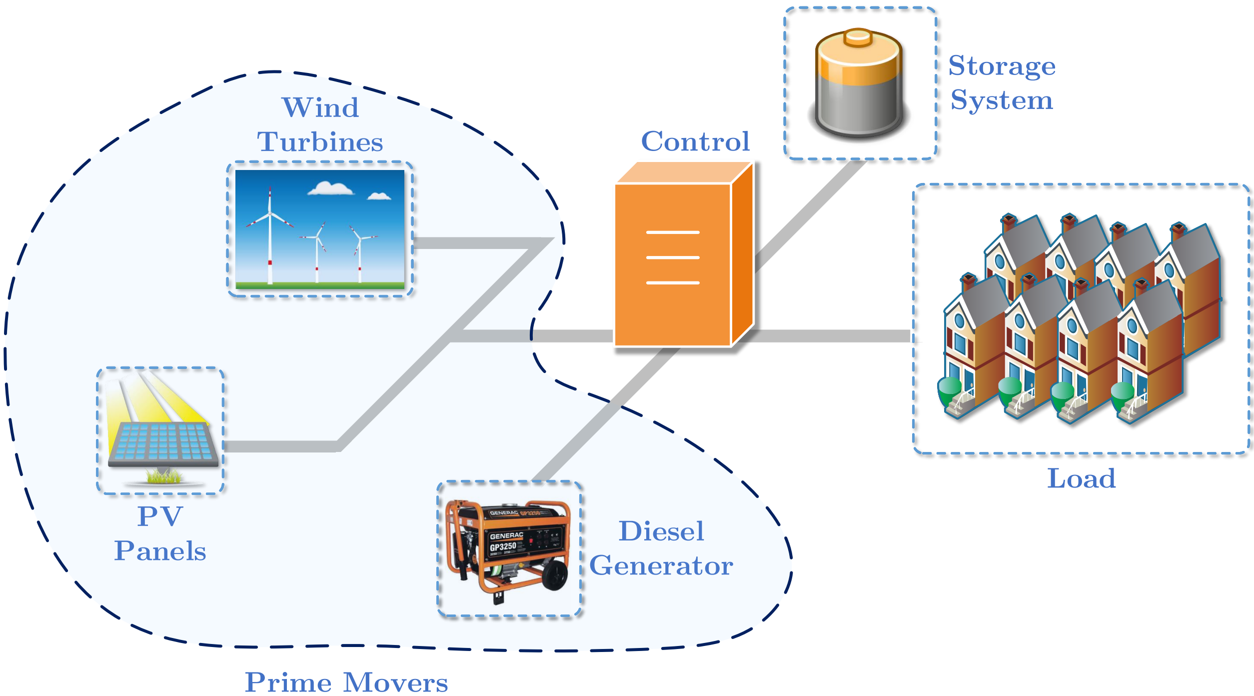

Fig. 2.1: Fundamental components of a MicroGrid.

ESSs contribute in a major way. In fact, they allow the energy storage when there is an over production and give the possibility to consume it when a power shortage occurs. Depending on the medium and on the conversion process, there are different storage technologies: chemical, electrochemical, mechanical, electrical and thermal storage. Nowadays the most used energy storage system is the pumped hydro [16], even though due to the spreading of DERs lead-acid and Lithium-ion batteries are gaining more and more popularity [16]. Furthermore, the researches around flywheels and supercaparcitors are generating interesting results [17], [18], [19]. For a more detailed overview of the existing storage systems and of their growth perspectives check [20],[21].

Moving forward with the analysis of the basic elements in a MicroGrid, there are the loads. They can differ from each other depending on the power needed, i.e. a private house, a commercial building or a factory. Another way to distinguish the loads is the need of continuity of electricity. Just think about the differences between the needs of a private house or an hospital or a data center. In the last two cases the power supply must be guaranteed in order to ensure in the hospital case the possibility to assist the patient and be able to carry on a surgery; while in the data center case, a blackout can cause the loss of sensitive data. One more criterion to classify the loads is by their linearity. Indeed, if a load changes its impedance with the applied voltage, it is defined as non-linear. This implies that the current drawn by the load contains harmonics that make it non sinusoidal even when the non-linear load is connected to a sinusoidal voltage. Furthermore, the harmonic currents, interacting with the grid impedance, will cause voltage distortions [22].

The interactions between all the system components have to be coordinated so that the MG is able to satisfy the constraints about power quality, power exchange with the grid, safety etc. This is the duty of the control unit that, from a hardware point of view, can be either a Digital Signal Processor (DSP) or a Field Programmable Gate Array (FPGA). The choice of the hardware of the control unit depends on the size, the control complexity and the processing power needed by the MicroGrid.

An element that is significant and plays a key role but is not highlighted in Fig.2.1 is the protection system. Indeed, the presence of distributed energy sources in nowadays medium- and low-voltage network made necessary an upgrade of the protections used until now. This because in the past, the distribution system was conceived as a radial network, delivering power from the substations to the customers, resulting in a unidirectional power flow. In this system the coordination of the circuit brakers through the use of overcurrent relays, reclosers and fuses was clearly defined [23], [24]. Nowadays instead, the deployment of DGs implies that the distribution network is no longer radial but has become active. For these reason, different approaches from the protection point of view have been developed and are still a hot research topic as can be seen in [25], [26], [27].

Once the basic elements that characterize a MicroGrid have been analyzed, it is interesting to see how the Microgrid interacts with the main grid in the two possible cases, namely the Islanded and the Grid-Connected mode.

2.3 Microgrid Operation Modes

As mentioned in Sec.1.1, one of the peculiarities of the Microgrid is that it can operate either while connected to the grid or as an energy island. This thanks to the possibility of using the VSI in the so called Voltage Controlled Mode (VCM) and Current Controlled Mode (CCM). When operating in VCM, the output voltage of the VSI is controlled, modulating its amplitude and frequency. In the CCM instead, the output current is regulated to the reference value. Furthermore the transition from one operational mode to the other can be done seamlessly. In this section the features of both operating modes are described.

2.3.1 Islanded Mode

When the Microgrid is not connected to the main grid, it is said to be in islanded mode. There are different scenarios where the islanded operation can be particularly advantageous. One of them is the electrification of places geographically difficult to reach or where the distance from the main grid is so big that the costs of the grid connection are too high compared to the incomes for the Distribution System Operator (DNO). In this case, the islanded operation is the best option in order to give access to electricity to the customers.

Another interesting scenario when the islanded-mode is not only advantageous but even crucial, is when a grid fault occurs. In this case, through the continuous monitoring of the grid status, the STS detects the extraordinary condition and disconnects the MG from the main grid, assuring the continuity of supply to the local loads and protecting distributed generators and storage systems. Doing so, the grid reliability is improved as well as its capability to reduce the number of consumers that experience the voltage outage.

It is worth to notice that the STS opens and lets the MG starts the islanded operation not only when a fault occurs, but also when the grid is weak, guaranteeing the power quality needed by the loads to work properly.

Following up on the correct operations of loads and generators, when in islanded mode, the Microgrid has to carry out duties that normally are pursued by the main grid:

- Voltage and frequency control so that both are within the limits. The typical accepted deviation for the voltage from its nominal value is ± 5% while for the frequency is ±2%;
- Power balance. This means that the amount of power produced by the DERs has to match with the amount of power needed by the loads. If there is a mismatch and there is an overproduction, ESSs can be a good solution. Nevertheless, if there is an underproduction, the voltage will drop, causing power outages and eventually a blackout;

- Power quality. This aspect is fundamental when it comes to supply the loads. In fact if the voltage supplied is not within the voltage and frequency limits above mentioned and its Total Harmonic Distortion (THD) is higher of a threshold value, typically 5%, then the loads can malfunction, fail prematurely or not operate at all.

In order to be able to ensure the above mentioned properties, there is the need to use some interface inverters for the distributed generators in the Microgrid in voltage controlled mode: the output voltage of each converter is modulated in amplitude and frequency (staying within the imposed thresholds), in order to provide the requested power.

In this way, even though some DERs' work in Current Controlled Mode (CCM), i.e. PVs and small wind turbines, in order to extract the maximum power from their energy source, the respect of the voltage amplitude and frequency thresholds is assured by the VSIs working in VCM.

2.3.2 Grid-Connected Mode

When the Microgrid is in grid-connected mode, it can either import power from the main grid or supply power to the distribution network, acting as a controllable load or as a controllable source. Further, the main utility grid imposes the active and the reactive power flow of the Microgrid so that the power imported from the grid is minimized. Then, these commands are managed by the MG's control unit and, by mean of communication buses, given to the DERs according to their power ratings. The goal is to produce most of the power *in loco* in order to reduce the burden on the distribution grid and consequently the losses in the energy transmission.

2.4 Control Approaches

For Microgrids, there are two main categories of controliling them: centralized and decentralized. In the centralized approach, all the information are sent to a central controller by means of high speed communication. Furthermore, the central controller performs all the calculations and consequently commands the control actions for each DG. On the contrary, in the decentralized control each unit has its own controller that performs calculations and gives control commands based on local measurements to the unit is in charge of, without being aware of the control actions taken by the other units [28].

2.4.1 Centralized Approaches

The employment of a centralized approach in the control of a Microgrid can be beneficial under several aspects. Indeed, a centrally controlled MG is easier to operate for the MG owner as all the actions that need to be taken are pursued by a central controller. In fact, after the data collection from all the components in the MG such as DERs, ESSs and eventual controllable loads and an analysis of the energy prices in the market, the central controller performs all the calculations in order to optimize the energy production and consumption inside the MG and the power exchange with the main grid. Further, the Microgrid central controller has also to act in order to meet the power quality requirements given by the grid codes.

The above mentioned characteristics make the centralized approach particularly suitable when:

- The owners of the DERs and the loads are pursuing common goals and want to reach them through cooperation;
- The MG's components are concentrated, i.e. in industrial or commercial Microgrids.

However, when the DERs are dispersed, there is the need of high bandwidth communication in order to guarantee good system dynamic response. This can be difficult to realize or, if possible, has a high cost. Furthermore, also the system reliability is decreased by the use of a centralized control since if the central controller experiences a fault, the whole MG won't be able to work.

Among the most known centralized control methods there are:

- Master & slave: on one inverter, in VCM, there is the central controller (master) that performs all the calculations and gives the power, voltage and frequency commands to the other inverters(slaves), in CCM. If the master fails, a slave unit will become the master, in order to avoid the system overall failure [29],[30];
- Average Load Sharing: the average current is sensed by means of a single wire with a properly chosen resistor connected to the current sensor for each converter.

In this case low-bandwidth communication can be used, but the current harmonics can circulate [31];

- Circular chain control (3C): the current reference of each module is taken from the module before, after sensing the inductor current, forming a control ring [32].

2.4.2 Decentralized Approaches

Unlike the centralized approaches, when the Microgrid is controlled in a fully decentralized way, each DG and ESS has its own controller that works independently, based just on local measurements. As a consequence, the distributed energy sources have plug-and-play capability, since they do not create any disturbance to the other DGs, increasing the reliability of the system. Nonetheless, a fully decentralized approach is not feasible for the control of several DGs due to the strong coupling between the operations of the units in the system. Therefore, a minimum level of communication in order to coordinates the operations of the inverters is needed [33].

A good compromise between the fully decentralized and the fully centralized approaches is the hierarchical control. It is structured in three levels, namely primary, secondary and tertiary. They differ from each other based on the speed of the response and their duties. The employment of the hierarchical control makes the integration of dispersed DERs possible by means of low bandwidth communication, increasing also the system reliability and redundancy [33]. Furthermore, the plug-and-play characteristic ensured by the decentralized approach can be achieved since there are higher control levels that take of the coupling between the operations of the units in the system.

In Fig.2.2 the general structure of the hierarchical control is presented, together with a brief overview of the main duties of each control level.

Primary Control

The primary control, or also known as local control, is the lowest level in the hierarchy. Its response relies solely on local measurements, without any need of communication. As basic level control, it has the fastest response in order to share the load among the paralleled dispatchable units based on their rated power. Furthermore, it has to have islanding detection capability and is also responsible for the improvement of voltage stability and for the reduction of circulating currents that may occur when the converters are connected in parallel [13], [34].

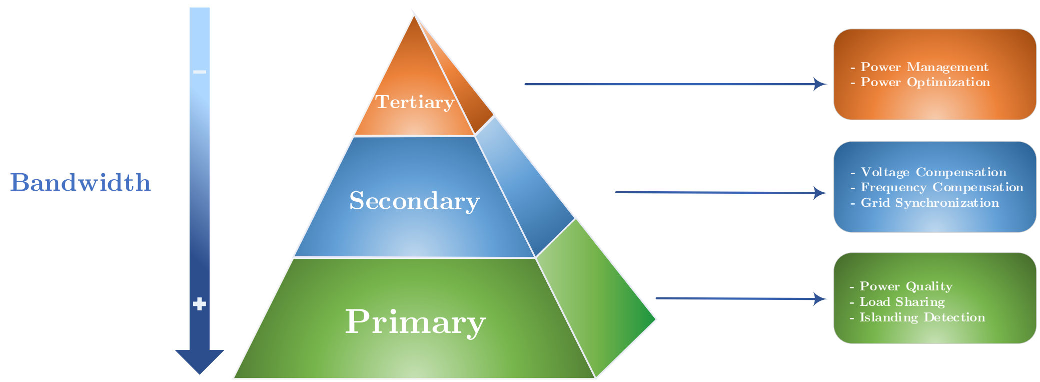

Fig. 2.2: Hierarchy of the control, with the duties of each level together with a qualitative representation of the bandwidth needed.

Among the control strategies for the primary level, the most known is the droop control, where the voltage amplitude and frequency are regulated based on the requested power, simulating the inertia of the synchronous generators in the transmission system [35].

Secondary Control

The secondary control has lower bandwidth with respect to the primary control, in order to decouple the two dynamics, but also to reduce the communication speed and to have enough time to perform all the calculations. Indeed, it compensates the voltage and frequency deviations caused by the primary control and performs the grid synchronization [36], [37]. Moreover, the secondary control can also act as the Energy Management System, taking care of power flow and power quality within the MG, as it is the highest control level when the MG is in islanded mode [33].

Tertiary Control

The last, and also the slowest level of control is the tertiary control. Indeed its control actions take place in the range of minutes. This level performs the power regulation when the Microgrid is connected to the grid. Furthermore, the power references given to the secondary control can be calculated based on an optimal analysis focused on the market prices, the weather forecasting (when sources with stochastic behavior are employed, e.g. PVs) and on the agreement between the customer and the grid operator [14], [38], [39].

HIERARCHICAL CONTROL

Chapter 3

Primary Control

3.1 Introduction

This is the lowest level in the control hierarchy, where the power sharing, the voltage and frequency control and the plug and play capability are achieved. In Fig.3.1 the main control blocks are depicted. The purpose of this chapter is to analyze and design first the inner loops, namely the current and the voltage loops. After this, it is described how the droop control works, its pros and cons and how its coefficients are calculated. The chapter ends with the the description of the synchronization loop.

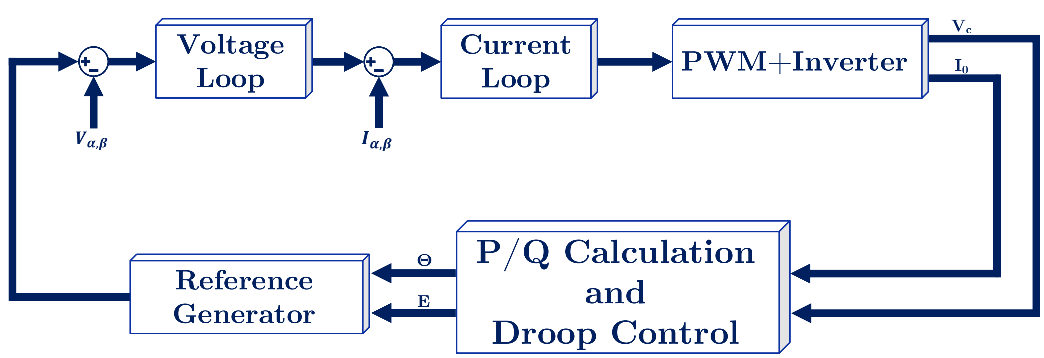

Fig. 3.1: Hierarchy of the control, with the duties of each level together with a qualitative representation of the bandwidth needed.

3.2 Voltage and Current Loops

When the nested loops control approach is used, the innermost loop has the fastest response, and consequently the highest bandwidth. The outer the loop, the slower the response. Therefore, the current loop has to have the highest bandwidth. In this project for the current loop a Proportional gain has been used, since the voltage loop is fast enough to ensure that the system works properly. For the voltage loop a Proportional+Resonant (PR) controller has been used. This choice has been made due to the ideally infinite gain at the resonant frequency ω_0 in the open loop bode diagram of the controller. Thanks to this property, the PR is able to track also sinusoidal signals with no steady-state error [40]. Moreover, compared to the classical PI controller, in the PR is more straightforward to implement the compensation of harmonics when needed, as can be seen from [41] and [42]. In the equation below is show the general structure of a PR, for sake of completeness, where ω_0 is the resonance angular frequency.

$$G_{PR}(s) = K_p + \frac{K_i s}{s^2 + \omega_0^2} \tag{3.1}$$

3.2.1 Current Loop

The design procedure of the current loop, whose structure is shown in Fig.3.2, where K_{PWM} is the gain of the PWM and is equal to $\frac{V_{DC}}{2}$, has been carried out as follows.

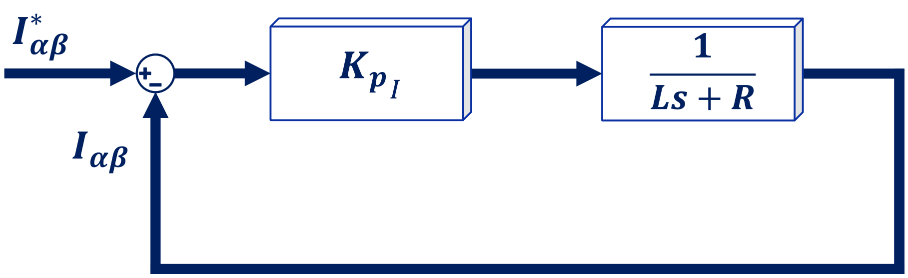

Fig. 3.2: Control structure of the P-based current loop.

First the closed-loop transfer function is derived:

$$CL_i(s) = \frac{G_i(s) K_{PWM} G_p(s)}{1 + G_i(s) K_{PWM} G_p(s)} \tag{3.2}$$

where $G_i(s) = K_{p_I}$ is the transfer function of the current controller and $G_p(s) = \dfrac{1}{Ls+R}$ is the transfer function of the plant.

After this, the cutoff frequency of the closed loop is set to be a fifth of the switching frequency. In order to fulfill this specification, the module of $CL_i(s)$ is calculated as:

$$|CL_i(s)| = \frac{K_{p_I} K_{PWM}}{\sqrt{\omega^2 + L^2 + (K_{p_I} K_{PWM} + R)^2}} \tag{3.3}$$

Then, since the bandwidth of the system is defined as the frequency where there is a decrease of $3dB$ in the Bode response of the magnitude, the module of $CL_i(s)$ is set to be equal to $\frac{1}{\sqrt{2}}$ at the defined closed loop cutoff frequency ω_c. After this, the proportional gain of the current controller can be derived as:

$$K_{p_I} = \frac{K_{PWM} R + \sqrt{K_{PWM}^2 R^2 + (\omega_c^2 L^2 + R^2) K_{PWM}^2}}{K_{PWM}^2} \tag{3.4}$$

In Fig.3.3 is shown the bode plot of the open loop when the designed controller is applied.

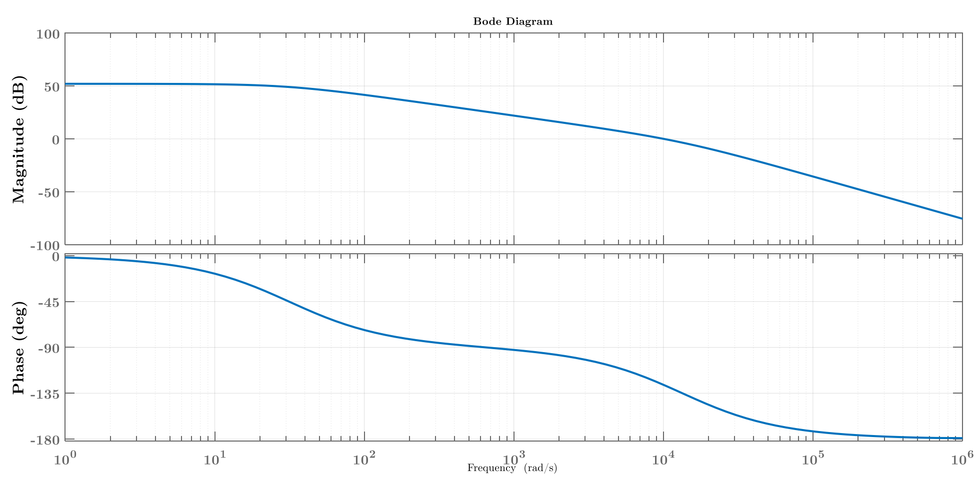

Fig. 3.3: Bode plot of the current loop obtained using a P controller with $K_{p_I} = 0.0698$.

3.2.2 Voltage Loop

For what regard the second innermost loop, namely the voltage loop, its control structure is shown in Fig.3.4. The design of the voltage controller has been carried out following the procedure described in [43] used for the PI tuning. Indeed, as stated in [40] and in [44], the PR controller is basically equivalent to a Proportional Integral (PI) controller but in a stationary reference frame.

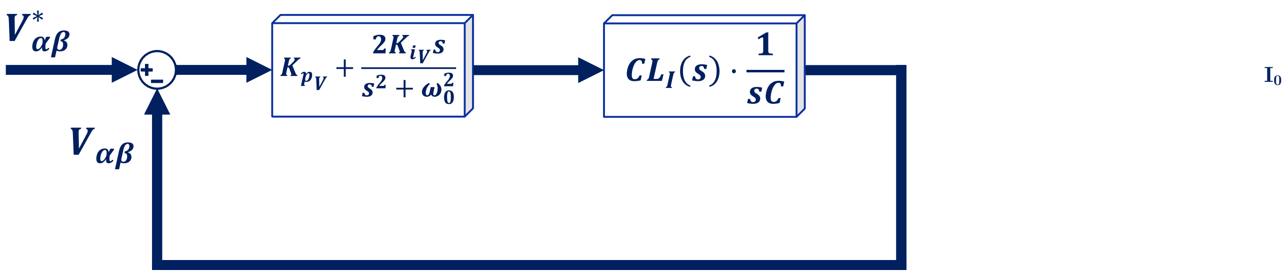

Fig. 3.4: Control structure of the PR-based voltage loop, where $CL_I(s)$ represents the closed-loop transfer function of the current loop.

First, considering the plant transfer function $G_p(s)$ (taking into account also the effects of the current controller), it is evaluated at what angular frequency ω_1 the next relation is satisfied:

$$\angle G_p(j\omega_1) = -180^\circ + \phi_m + 5^\circ \tag{3.5}$$

where ϕ_m is the desired phase margin. After this, the proportional and resonant terms of the controller are obtained as follows:

$$k_{pv} = \frac{1}{|G_p(j\omega_1)H(j\omega_1)|} \tag{3.6}$$

$$k_i v = 0.1\,\omega_1\,k_{pv} \tag{3.7}$$

The result of the voltage loop design is shown in Fig.3.5, where the bode plot of the voltage open loop is depicted.

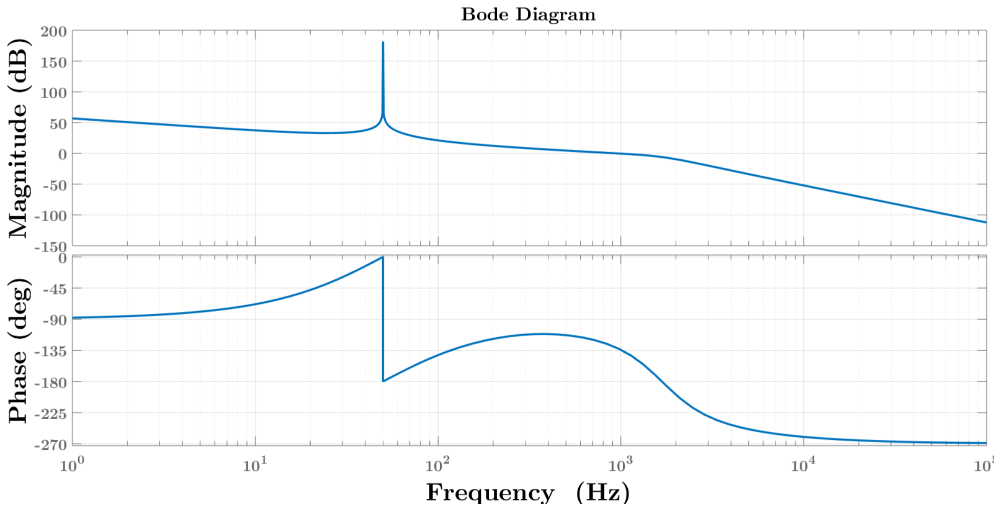

Fig. 3.5: Bode plot of the voltage loop obtained using a PR controller with $K_{p_V} = 0.0433$ and $K_{i_V} = 25.85$. The phase margin is equal to 48.7°, validating the design procedure.

3.3 Droop control

On the primary control level, the core is represented by the droop control that gives the possibility of power sharing without the use of communication links. The idea behind the droop control is to emulate the behavior of the synchronous generators that changes the frequency and amplitude of the voltage, based on the load [45]. Indeed, since the power electronic interface is inertia-less, a control able to adapt itself when the load changes has to be implemented. This can be achieved adjusting the output voltage frequency and amplitude, as can be seen from Fig.3.6: an increase in the power demand implies a decrease in the voltage frequency or amplitude, whether the increase is in the active or reactive power respectively.

In order to understand how the the power is related to the change in the amplitude and in the frequency, first the general equations of the power have to be written. Let's consider the simple system in Fig.A.1, composed by a generator with amplitude E and phase θ, a voltage V at the PCC with no phase shifting and a feeder impedance with module Z and phase φ.

The equations of the active and the reactive power considering this system can

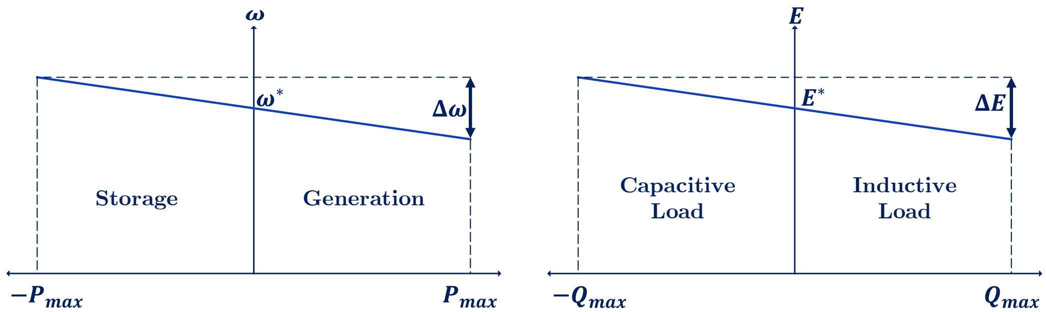

(a) $P-\omega$ droop function. **(b)** $Q-E$ droop function.

Fig. 3.6: Droop of voltage and frequency based on the power request.

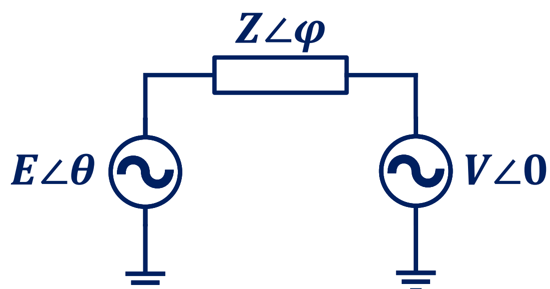

Fig. 3.7: Connection of a DG inverter to the grid through a complex feeder.

be written as:

$$P = \left(\frac{EV cos\theta}{Z} - \frac{V^2}{Z}\right) cos\varphi + \frac{EV sin\theta}{Z}\ sin\varphi \tag{3.8}$$

$$Q = \left(\frac{EV cos\theta}{Z} - \frac{V^2}{Z}\right) sin\varphi - \frac{EV sin\theta}{Z}\ cos\varphi \tag{3.9}$$

The derivation of these two equations can be found in Appendix A. As can be seen, there is no decoupling between P and Q. However, two assumptions can be made. First, the output impedance can be assumed mainly inductive due to the inverter filter and to the impedance of the power lines [34], [46]. This way $Z = X$ and $\varphi = 90°$. Second, the phase angle difference between E and V is normally small. Therefore

$sin\theta \approx \theta$ and $cos\theta \approx 1$. This way, the active and reactive power equations become:

$$P = \frac{EV}{X}\theta \tag{3.10}$$

$$Q = \frac{V}{X}(E - V) \tag{3.11}$$

As can be seen, now the the active power is proportional to the phase angle and the reactive power is proportional to the voltage vectors magnitude difference $(E - V)$. Once the decoupling between active and reactive power is achieved, the droop control functions can be defined:

$$\theta = \theta^* - G_P(s)(P_{LPF} - P^*) \tag{3.12}$$

$$E = E^* - G_Q(s)(Q_{LPF} - Q^*) \tag{3.13}$$

where θ^* is the reference angle, P^* and Q^* are the reference of the active and of the reactive power respectively while P and Q are the measured one. The power calculation is performed in the $\alpha - \beta$ frame with the well known relations:

$$p = v_{c\alpha} \cdot i_{0\alpha} + v_{c\beta} \cdot i_{0\beta} \tag{3.14}$$

$$p = v_{c\beta} \cdot i_{0\alpha} - v_{c\alpha} \cdot i_{0\beta} \tag{3.15}$$

After the power calculation a low pass filter with crossing angular frequency $\omega_{c_{LPF}}$, in order to eliminate the ripple and make it a DC value so that a PID can be used. Finally, E^* is the reference voltage while E is the measured one. In the equations $G_P(s)$ and $G_Q(s)$ are the droop controller transfer functions, whose equations are shown in eq.3.16 and eq.3.17.

$$G_P(s) = k_{pP} + \frac{K_{iP}}{s} + k_{dP}s \tag{3.16}$$

$$G_Q(s) = k_{pQ} + \frac{K_{iQ}}{s} + k_{dQ}s \tag{3.17}$$

Has to be noticed that it has been used the angle instead of the frequency since it allows a better dynamic performance [6], [47]. Furthermore, the reference powers are set to zero during islanding operations since the amount of power drawn from the inverters is set by the loads, while when connected to the grid the P and Q are set to their nominal values. Regarding the controllers, K_{i_P} and K_{p_Q} are called static droop coefficients while K_{p_P} is the transient droop term and it provides a virtual inertia to the system. The static droop coefficients can be calculated as follows:

$$K_{i_P} = \frac{\Delta f}{\Delta P} \tag{3.18}$$

$$K_{p_Q} = \frac{\Delta V}{\Delta Q} \tag{3.19}$$

where Δf is the maximum frequency variation allowed (typically $\pm 2\%$), ΔV is the maximum voltage amplitude deviation (typically $\pm 5\%$). The exact frequency and voltage deviations vary based on the country, e.g. $\pm 0.1\,Hz$ in Nordel (North of Europe) or $\pm 0.3\,Hz$ in the Union for the Coordination of Transmission of Electricity(Continental Europe) [48]. Finally, ΔP, ΔQ are the nominal active and reactive power respectively. When the Microgrid is connected to the grid, the derivative action of $G_P(s)$ and the integral and derivative actions of $G_Q(s)$ ensure that the power flow follows the reference with no steady-state error. The tuning of these terms can be done following the procedure described in [49], where first an analysis based on the small signal model of the system is carried out. After this, the coefficients can be calculated looking at the poles placement and considering the desired damping and transient response.

Even though the performance of the system is improved using Proportional Integral Derivative (PID) controller in the droop functions, the droop control has inherently some drawbacks. Indeed, when the first assumption regarding the output impedance is not satisfied, which is the case in LV Microgrids where the line impedance is mainly resistive, then active and reactive power are not decoupled anymore. In this case, one solution is the virtual impedance. Moreover, in order to obtain a good power sharing the droop coefficients can be increased, but at expense of degrading the voltage regulation. As a consequence of this trade-off, the systems has a slow transient response and has poor performances in terms of harmonic load sharing when non linear loads are supplied [50], [51], [52].

3.4 Synchronization Loop

When connecting two or more VSIs together or connecting the MG to the main grid, a synchronization loop is needed. Indeed, if the voltages are not synchronized both in amplitude and frequency, the mismatch causes reactive power flow, problems in the proper working of equipment and finally instability. Hereafter the block diagram of the synchronization method in the α, β frame used in [6] is shown. After it, its working principles are described.

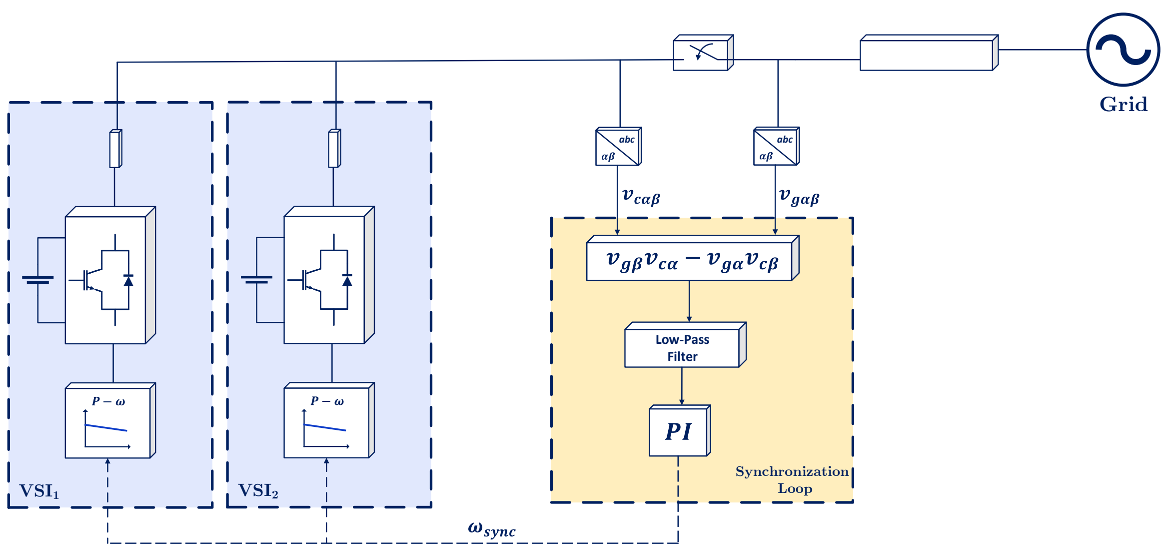

Fig. 3.8: Schematic of the synchronization loop when the synchronization between the grid and the Microgrid is performed.

When the two voltages, namely v_1 and v_2 are synchronized, the following equation is satisfied:

$$< v_{1\beta} \cdot v_{2\alpha} - v_{1\alpha} \cdot v_{2\beta} >= 0 \tag{3.20}$$

where $< x >$ is the average value of the variable x over the nominal frequency. Here v_1 is taken as reference voltage, being it either the grid voltage or a VSI voltage.

Following the flow in Fig.3.8, the output signal ω_{sync} is calculated as:

$$\omega_{sync} = (v_{1\beta} \cdot v_{2\alpha} - v_{1\alpha} \cdot v_{2\beta}) \frac{\omega_c}{s + \omega_c} \frac{K_{p_{sync}} s + K_{i_{sync}}}{s} \tag{3.21}$$

where $K_{p_{sync}}$ and $K_{i_{sync}}$ are the coefficients of the PI and w_c is the cutoff angular frequency of the low-pass filter. The resulting output signal ω_{sync} is then sent to the VSIs in order to synchronize them either with another VSI or with the main grid adjusting their $P-\omega$ droop function. This way the voltage vectors will have the same frequency. Has to be noticed that instead of using phase or time-domain information, which would need critical high-speed communication, the use of frequency data allows the deployment of low-bandwidth communication.

To avoid a mismatch in the voltages' amplitude, a similar approach, shown in Fig.3.9 can be used. It consists of a simple subtraction between the d-component of v_1 and v_2. They have been calculated using a Park transformation with the angle of each voltage, extracted by a Phase Locked Loops (PLLs), whose parameter are calculated as in [53]. The error than is fed to a PI that gives as output a voltage deviation dv that has to be applied to the VSIs.

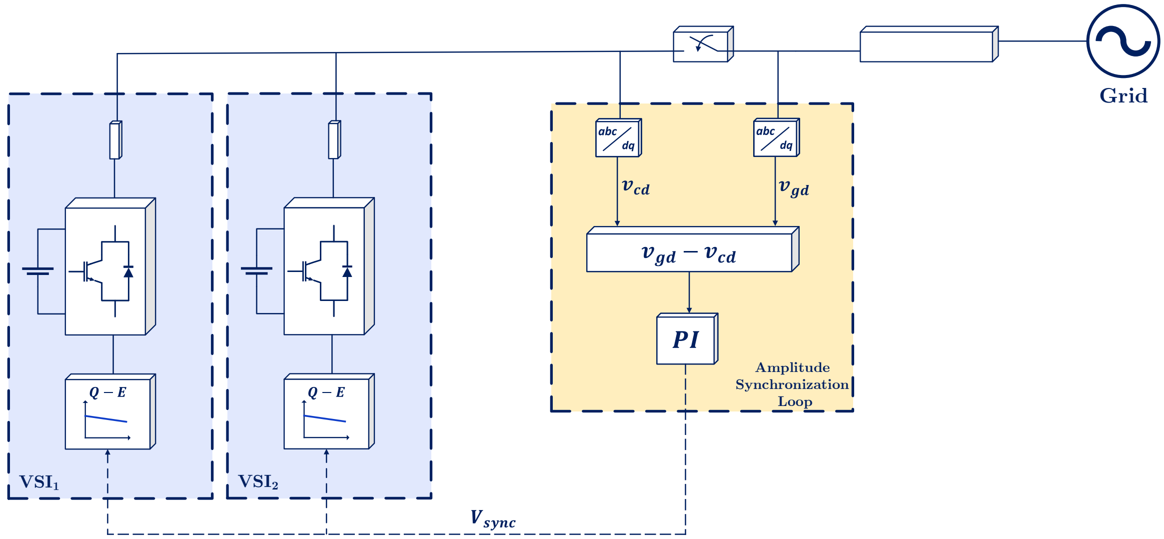

Fig. 3.9: Schematic of the synchronization loop when the synchronization between the grid and the Microgrid is performed.

Chapter 4

Secondary Control

4.1 Introduction

The droop control, when there is a variation in the load, produces a deviation in the frequency and in the amplitude from the nominal values. To overcome these issues, a secondary control can be introduced [35], [6]. The purpose of such control is to emulate a compensation for the inertia provided by the synchronous generators in the grid [54]. In this chapter two approaches are studied: the standard centralized secondary control and the decentralized control.

4.2 Centralized Secondary Control

In the centralized approach, the measured voltage and frequency of all DGs are collected by a central controller that, after the calculations, gives the frequency and voltage deviations commands to the primary control of each DG, as can be seen from Fig.4.1.

4.2.1 Frequency Restoration

In order to remove the steady-state error in the frequency a PI is used. Furthermore, the same criteria for the bandwidth applied before is used, so that the dynamics of the different loops are decoupled. Here the frequency PI parameters have been calculated following the procedure described in [6]. First, the compensator equation can be written

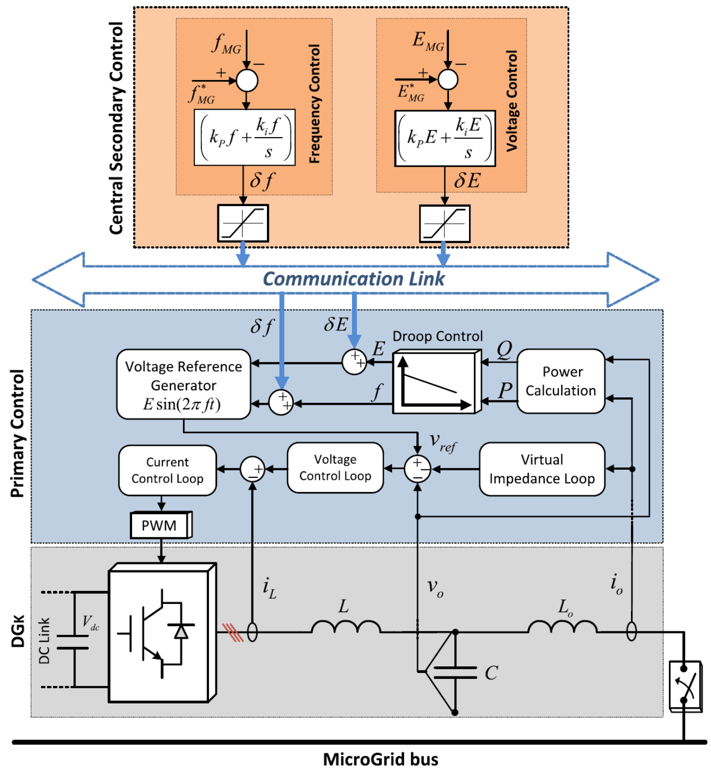

Fig. 4.1: Block diagram of the centralized secondary control [56].

as:

$$\omega_{rest} = K_{p_f}(\omega_{MG}^* - \omega_{MG}) + K_{i_f} \int (\omega_{MG}^* - \omega_{MG})\, dt \tag{4.1}$$

where K_{p_f} is the proportional term while K_{i_f} is the integral one, and (ω_{MG}^* and ω_{MG}) are the reference and actual values of the MG angular frequency respectively. Is worth to notice that ω_{rest} has to be limited so that the frequency thresholds are respected.

To determine the compensator values, the block scheme in Fig.4.2 is used.

From this scheme, the model in Eq.4.2 can be obtained.

$$\omega_{MG} = \frac{G_{f_{sec}}(s)G_d(s)}{1 + G_{f_{sec}}(s)G_d(s)G_{PLL}(s)}\omega_{MG}^* - \frac{K_{i_P} G_{LPF}(s)}{1 + G_{f_{sec}(s)G_d(s)G_{PLL}(s)}}P \tag{4.2}$$

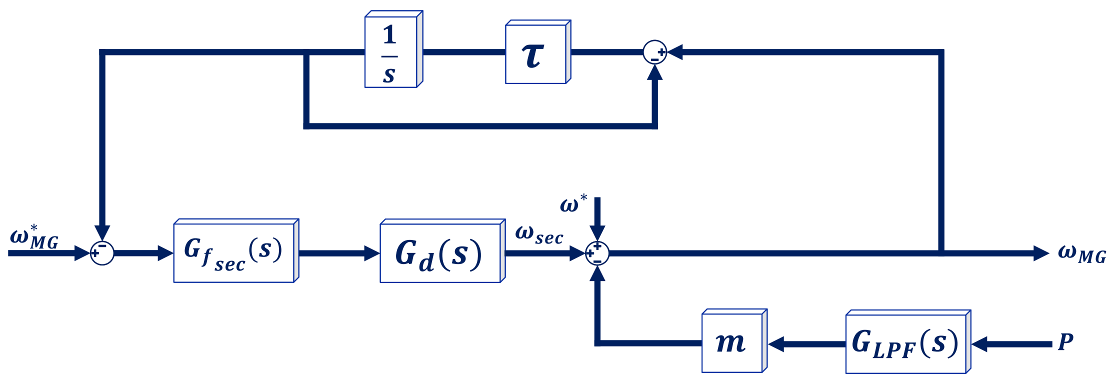

Fig. 4.2: Block diagram of the secondary frequency restoration action.

Below, all the transfer functions expression are shown.

$$G_{f_{sec}}(s) = K_{p_f} + \frac{K_{i_f}}{s} \tag{4.3}$$

$$G_{PLL}(s) = \frac{1}{\tau s + 1} \tag{4.4}$$

$$G_d(s) = \frac{1}{s + 1.5\omega_s} \tag{4.5}$$

$$G_{LPF}(s) = \frac{\omega_c}{s + \omega_c} \tag{4.6}$$

where $G_{f_{sec}}(s)$ is the transfer function of the PI, $G_{PLL}(s)$ is the low-pass filter approximation of the PLL dynamic, $G_d(s)$ is the transfer function of the delay introduced by the communication from the secondary control to the primary level and finally $G_{LPF}(s)$ is the low-pass filter transfer function.

Once the model is defined, it is possible to determine the frequency compensator parameters considering the step response based on the closed-loop transfer function $P - to - \omega_{MG}$ when a change in the active power occurs. In this project the effect of the delay has not been considered. For a deeper understanding on how the delay influences the response and how to consider it in the stability analysis, see [55].

4.3 Voltage Restoration

The steady-state error in the amplitude can be removed by use of a PI controller, like in the case of frequency restoration. The considerations regarding the decoupling between the droop control loop and the secondary control loop are valid also in this case. The voltage compensator form can be derived from the following equation:

$$E_{rest} = K_{p_E}(E^*_{MG} - E_{MG}) + K_{i_E} \int (E^*_{MG} - E_{MG})\, dt \tag{4.7}$$

where K_{p_E} and K_{i_E} are the voltage restoration PI proportional and integral part respectively, E^*_{MG} is the reference voltage of the Microgrid while E_{MG} is the measured one.

Now, following the same procedure as for the frequency restoration, first from the block diagram in Fig.4.3 the following model can be obtained:

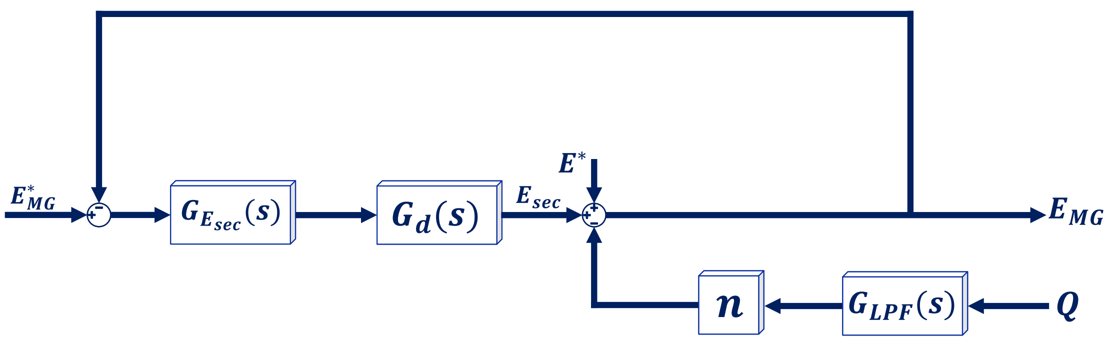

Fig. 4.3: Block diagram of the secondary voltage restoration action.

$$E_{MG} = \frac{G_{E_{sec}}(s)G_d(s)}{1 + G_{E_{sec}}(s)G_d(s)} E^*_{MG} - \frac{K_{p_Q} G_{LPF}(s)}{1 + G_{E_{sec}(s)G_d(s)}} Q \tag{4.8}$$

where $G_{E_{sec}}$ is the voltage restoration PI controller defines as follows:

$$G_{E_{sec}}(s) = K_{p_E} + \frac{K_{i_E}}{s} \tag{4.9}$$

Finally, the parameters of the controller can be designed considering the step response of the $Q - to - E$ transfer function.

4.4 Decentralized Secondary Control

Since in the centralized secondary control a MG central controller failure corresponds to a failure of the system, the distributed secondary control proposed in [56], whose structure is shown in Fig.4.4, is described. In this way, if an inverter fails, the others are still able to work. Another advantage of the distributed secondary control is that is needed lower communication bandwidth compared to the centralized one.

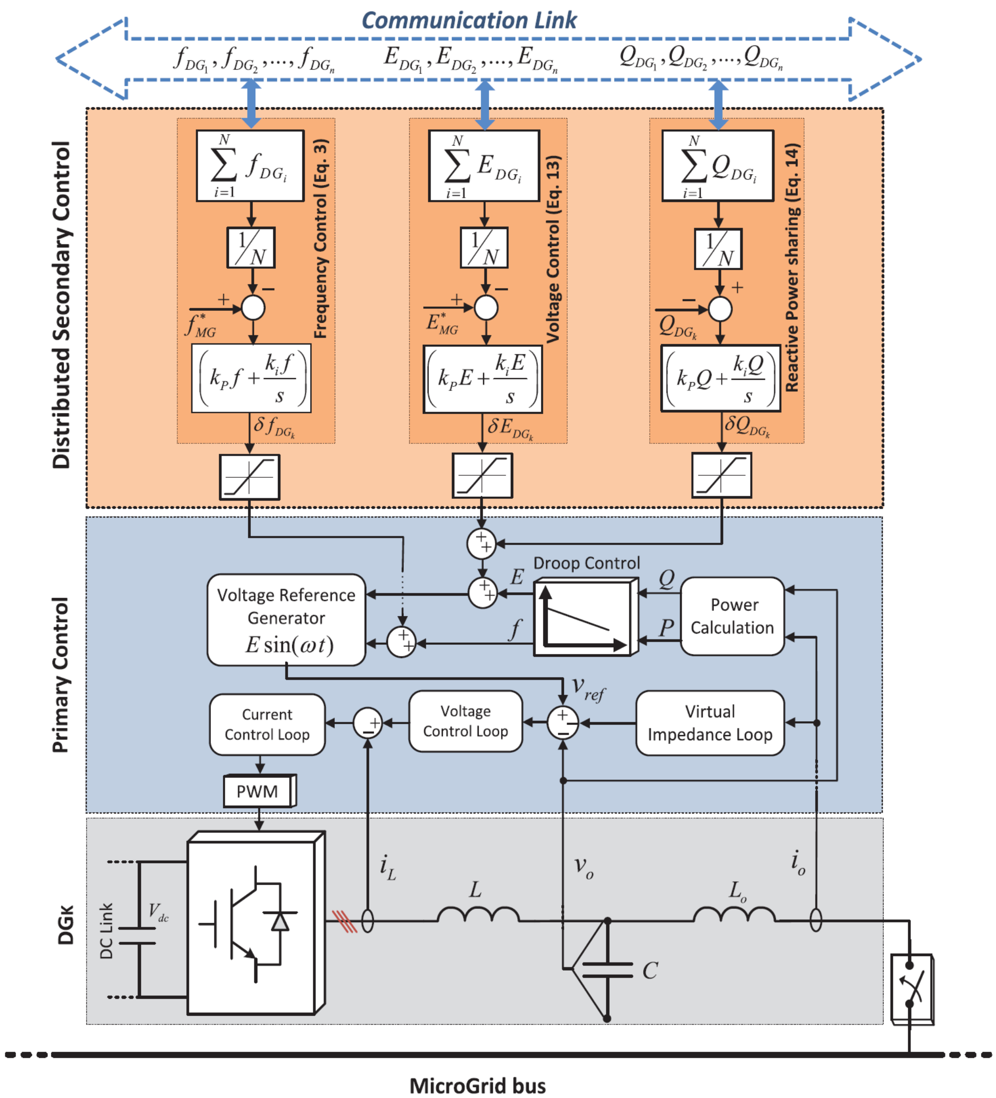

Fig. 4.4: Block diagram of the distributed secondary control [56].

4.4.1 Frequency Restoration

The frequency is restored to its nominal value using a PI controller as in the centralized method. The difference is that each DG measures the frequency every sample time, and sends the data to the other DGs. Then, the frequency information from the other DGs are averaged. Finally the frequency is restored giving a frequency command δf as follows.

$$\delta f_{DG_k} = K_{p_f}(f^*_{MG} - \overline{f}_{DG_k}) + K_{i_f} \int (f^*_{MG} - \overline{f}_{DG_k})\, dt \tag{4.10}$$

where K_{p_f} and K_{i_f} are the PI parameters, f^*_{MG} is the frequency set point of the Microgrid, δf_{DG_k} is the frequency control signal of the k-th DG and $\overline{f}_{DG_k}$ is the frequency average for all DGs and is defined as:

$$\overline{f}_{DG_k} = \frac{\sum_{i=1}^{N} f_{DG_i}}{N} \tag{4.11}$$

Here N represents the number of frequency measurements and n is the number of DGs.

According to [56], the transfer function of the system can be written as :

$$\Delta_f = 1 + G_{LPF}(s) \cdot G_P(s) \cdot \frac{1}{s} \cdot G + G_{PLL}(s) \cdot k_a \cdot G_{f_{sec}}(s) \tag{4.12}$$

Where

$$G_{LPF}(s) = \frac{1}{\tau_p s + 1} \tag{4.13}$$

$$G_{PLL}(s) = \frac{1}{\tau s + 1} \tag{4.14}$$

$$G_{f_{sec}}(s) = K_{p_f} + \frac{K_{i_f}}{s} \tag{4.15}$$

The calcultion of the controller parameters can be performed analyzing the eigen values of Eq.4.12.

4.5 Voltage Restoration and Q Flow Control

For what regards the voltage restoration, a similar approach as the one described for the frequency restoration can be used. The DG voltage is measured and the value communicated to the other DGs. The others DGs voltages are then averaged so that a voltage command can be given. The voltage restoration can be performed using the following controller:

$$\delta E_{DG_k} = K_{p_E}(E^*_{MG} - \overline{E}_{DG_k}) + K_{i_E}\int (E^*_{MG} - \overline{E}_{DG_k})\, dt \tag{4.16}$$

where K_{p_E} and K_{i_E} are the PI parameters, E^*_{MG} is the reference voltage of the Microgrid, δE_{DG_k} is the voltage control signal of the k-th DG and $\overline{E}_{DG_k}$ is the voltage average for all DGs and is defined as:

$$\overline{E}_{DG_k} = \frac{\sum_{i=1}^{N} E_{DG_i}}{N} \tag{4.17}$$

Due to the difficulties in the reactive power sharing in a Microgrid with a low R/X ratio, also a controller for the reactive power flow has been implemented. The controller has the following structure:

$$\delta Q_{DG_k} = K_{pQsec}(Q^*_{MG} - \overline{Q}_{DG_k}) + K_{iQsec}\int (Q^*_{MG} - \overline{Q}_{DG_k})\, dt \tag{4.18}$$

where K_{pQsec} and K_{iQsec} are the PI parameters, E^*_{MG} is the reference voltage of the Microgrid, δQ_{DG_k} is the voltage control signal of the k-th DG and $\overline{Q}_{DG_k}$ is the voltage average for all DGs and is defined as:

$$\overline{Q}_{DG_k} = \frac{\sum_{i=1}^{N} Q_{DG_i}}{N} \tag{4.19}$$

According to [56], finding the eigen values of the following characteristic equations, it is possible to calculate the parameters of both voltage and reactive power flow controllers.

$$\Delta_E = 1 + (G_{LPF}(s) \cdot G_Q(s) \cdot H) + (k_a \cdot G_{E_{sec}}(s)) \tag{4.20}$$

$$\Delta_Q = 1 + (G_{LPF}(s) \cdot G_Q(s)H) + (k_a \cdot H \cdot G_{Q_{sec}}(s)) \tag{4.21}$$

Chapter 5

Implemented MG Control Analysis

The aim of this chapter is to validate the control design described throughout the thesis with the simulation work, when applied to the scenario presented in Section 1.2, shown again in Fig.5.1 for ease of reference.

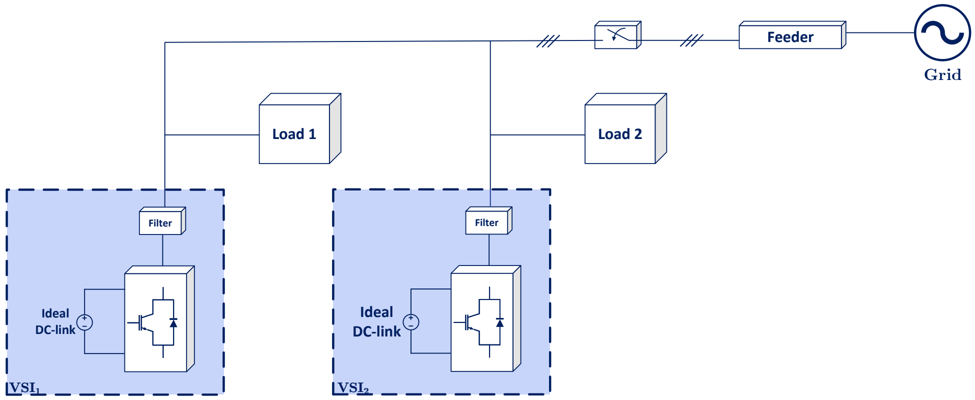

Fig. 5.1: Case scenario considered throughout the simulation work.

The parameters used in the simulations are summarized in Table 5.1. It is worth to notice that the LCL filter components have been designed following the procedure described in [57], when a 10% ripple on the maximum inductor current on a $10\,kW$ Inverter with a DC-link voltage of $650\,V$, a switching frequency of $10\,kHz$ and delta connected capacitors are considered.

Furthermore, since the control strategy is based on the control of the converter-side inductor current and on the voltage across the capacitor, L_2 can be seen as a feeder inductance and due to its quite high value, it can be comprehensive of both the inverter and the grid feeder, hypothesizing a stiff grid. This way, the R/X ratio is low enough to

Parameter	Symbol	Value
Grid Voltage	V_g	230 V
System Frequency	f	50 Hz
Converter-side Inductance	L_1	2.86 mH
Converter-side Resistance	R_1	0.0898 Ω
Grid-side Inductance	L_2	3.05 mH
Capacitor	C	3.32 μF
VSI_1 Load	Load 1	2 kW, 500 VAR
VSI_2 Load	Load 2	10 kW, 500 VAR

Tab. 5.1: System Parameters

justify the use of the droop control equations shown in Eq.3.10 and Eq.3.11. Moreover, since the focus has been on the control structure, voltage-controlled sources instead of actual VSIs have been used, without having to care about the problems related to the modulation or to the DC-link that may arise. Knowing all this, therefore, the analysis has been carried out first in the islanded mode scenario, using only the primary control when a load change and the connection of another inverter occur. After this, the grid-connected scenario has been taken into account, showing both the MG's capabilities to perform the transition seamlessly and to follow the power reference commands given by the main grid.

5.1 Islanded Mode

Before going through the evaluation of the system response from different points of view, first the parameters of both primary, secondary and tertiary control are shown in Table 5.2. Has to be noticed that the proportional gain of the current loop K_{p_I} has been decrease compared to the one obtained in the design phase, in order to make the system stable. One reason for this can be addressed to the fact that the design of the current controller has been carried out for an LC filter. Nevertheless, the interaction with the grid-side inductance, if not taken into account, may lead to the system instability. For what regards the gain of the voltage PR, it also has been decrease in order to ensure the decoupling between the voltage and the current loop dynamics.

The first thing to verify is that the inner loops are able to follow the given reference when a load step change occurs. From Fig.5.2 can be seen that the voltage loop is able to track the change in the voltage reference, avoiding any overshoot in the response.

Parameter	**Symbol**	**Value**
Primary Control		
Proportional Gain Current Loop	K_{p_I}	0.03
Proportional Gain Voltage Loop	K_{p_V}	0.0217
Integral Gain Voltage Loop	K_{i_V}	47
Proportional Gain Droop Frequency Control	K_{p_P}	1e-6
Integral Gain Droop Frequency Control	K_{i_P}	2e-5
Derivative Gain Droop Frequency Control	K_{d_P}	1e-6
Proportional Gain Droop Voltage Control	K_{p_Q}	1e-3
Integral Gain Droop Voltage Control	K_{i_Q}	5e-2
Derivative Gain Droop Voltage Control	K_{d_Q}	1e-4
Proportional Gain Frequency Synchronization Loop	$K_{p_\omega sync}$	4e-5
Integral Gain Frequency Synchronization Loop	$K_{i_\omega sync}$	1e-3
Proportional Gain Amplitude Synchronization Loop	$K_{p_A sync}$	0.1
Integral Gain Amplitude Synchronization Loop	$K_{i_A sync}$	5
Secondary Control		
Proportional Gain Frequency Restoration	K_{p_f}	0.001
Integral Gain Frequency Restoration	K_{i_f}	10
Proportional Gain Voltage Restoration	K_{p_E}	0.002
Integral Gain Voltage Restoration	K_{i_E}	10
Proportional Gain Q Control Distributed Secondary	$K_{p_Q sec}$	0.00001
Integral Gain Q Control Distributed Secondary	$K_{p_Q sec}$	0.001

Tab. 5.2: Parameters of all the levels of the hierarchical control.

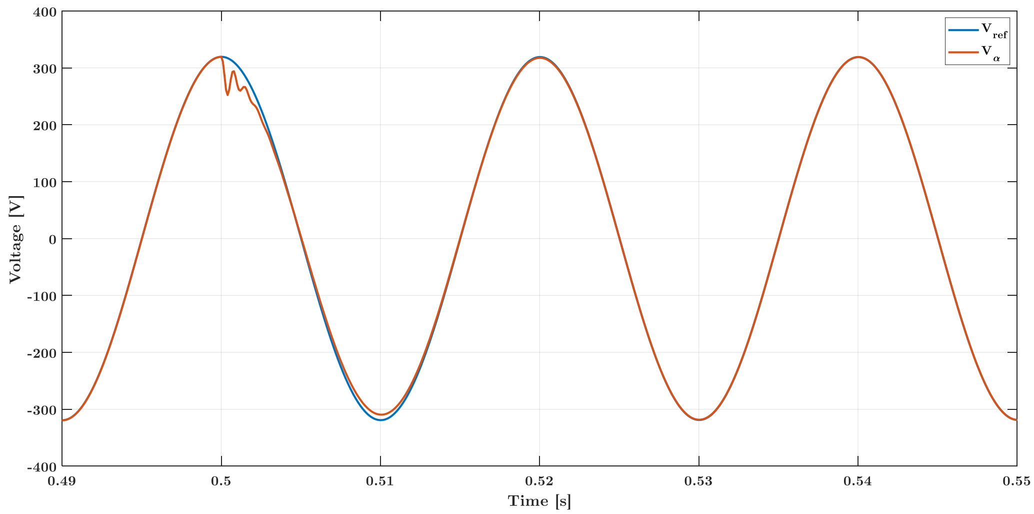

Fig. 5.2: Step response of the α component of the voltage when a step change in the load occurs.

Once the correct behavior of the inner loops has been achieved, in order to prove the primary control is working in the right way, the scenario described in Fig.5.3 has been set.

Fig. 5.3: Flow of the changes in the simulations scenario.

In Fig.5.4 both the active and the reactive power of the two VSI are shown. As can be seen from, when at 0.5 seconds another load of $2\,kW$ and $500\,VAR$ is introduced, the first inverter is able to follow the load change, even though there is some steady state error that can be due to the voltage and frequency deviations of the droop control. Simultaneously, the second inverter when supplying the second load, presents higher steady-state error especially in the reactive power. This errors can be addressed to the employment of a low-pass filter for the power calculations. Furthermore, the error in the reactive power is influenced also by the reactive power dissipated in the grid-side inductance and by the difference in the frequency between the nominal frequency of the load and the actual frequency of the inverter. Then, once the synchronization process between the two inverters ends, they are connected at 3 seconds. As can be seen, after some oscillations the VSIs are able to share the power equally, even when another load change of $2\,kW$ and $500\,VAR$ occurs at 6 seconds.

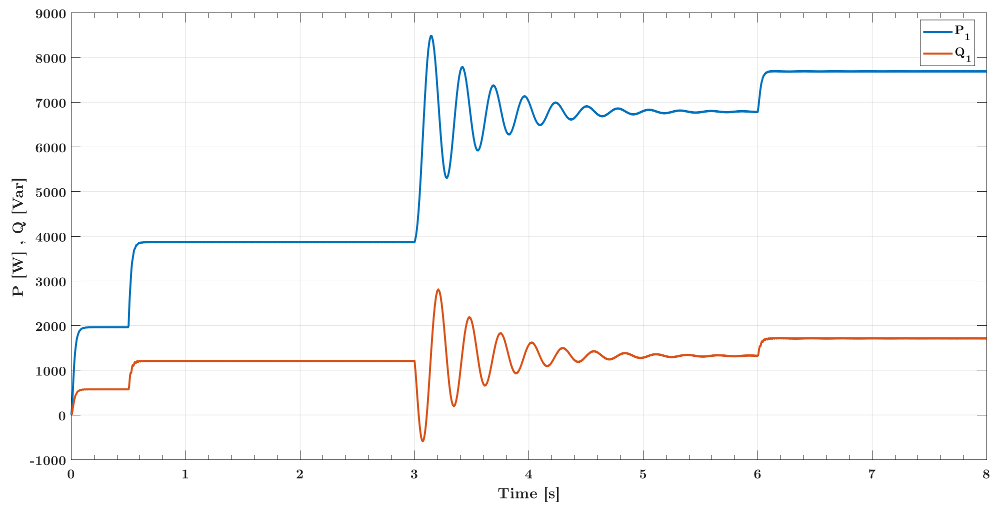

(a) Active and reactive power in the first inverter.

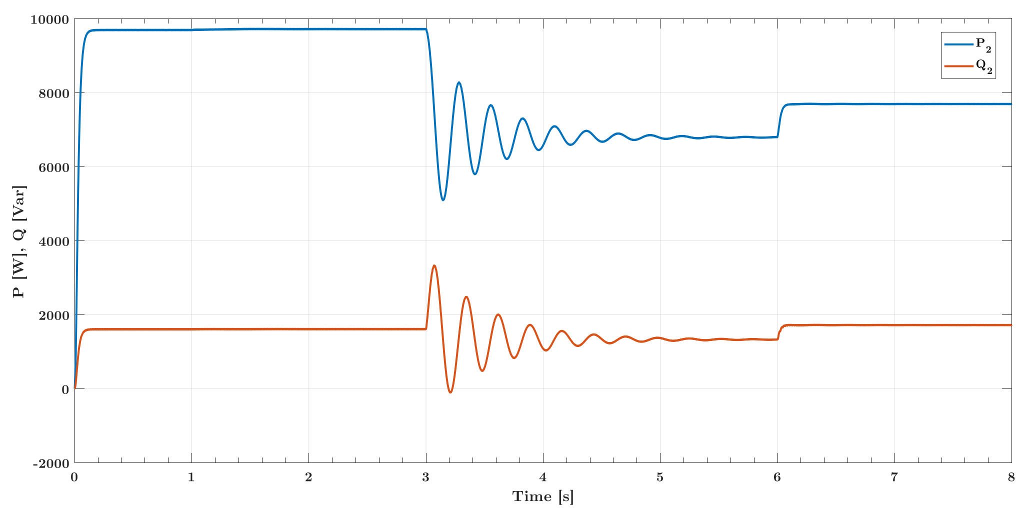

(b) Active and reactive power in the second inverter.

Fig. 5.4: Power changes of the two inverters.

A detail of the synchronization process between the two inverters can be seen in Fig.5.5, where are shown the synchronization errors in the frequency(Fig.5.5a) and in the voltage(Fig.5.5b).

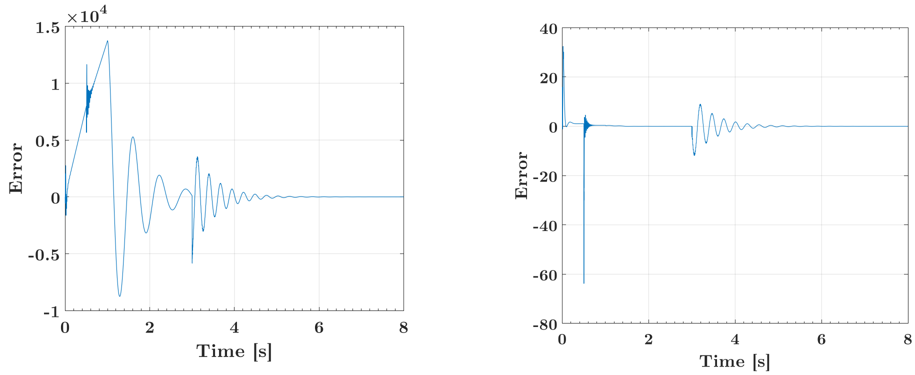

(a) Frequency error. **(b)** Voltage error.

Fig. 5.5: Synchronization errors in frequency and voltage in the two inverters.

As can be seen, the main difference is in the frequency due to the disparity in the active power between the loads supplied. Anyway, once the synchronization is done at 3 seconds, the VSIs need 2 seconds more to reach the zero error condition. This can be due to the fact that the closure of the breaker and consequently the introduction of the second inverter, can be seen as a perturbation from the first inverter point of view. Therefore, some time is needed so that the system reaches the steady-state.

For what regards the currents and voltages of the two inverters during the synchronization process, the currents in the first VSI have a peak that is not too high compared to the nominal value. This can be seen in Fig.5.6 where the three-phase voltages and currents of both inverters are shown. Furthermore, it is evident looking at the two inverters' currents how, after the synchronization, they are sharing the loads equally.

As above mentioned, besides the capability of the droop control to ensure the power sharing, its main drawbacks are the frequency and voltage deviations. These phenomena can be see clearly in Fig.5.7.

In order to overcome these deviations, the secondary control has been implemented in both centralized and decentralized way. From Fig.5.11 can be seen that when the centralized secondary control is activated at five seconds, both the frequency and the voltage are restored to their nominal value. Furthermore, it is demonstrated also that the system follows the reference values even when a change in the load occurs, at nine seconds.

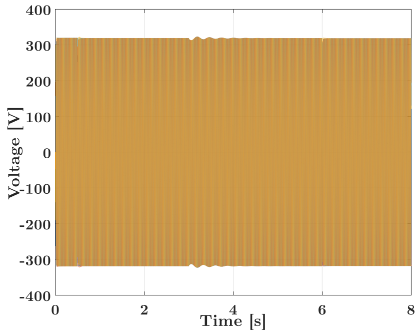

(a) Inverter one voltages.

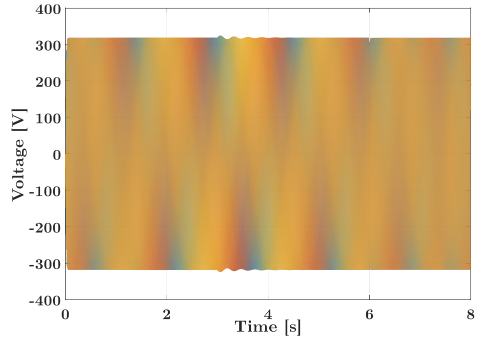

(b) Inverter two voltages.

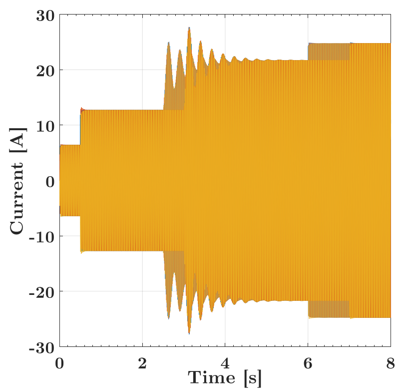

(c) Inverter one currents.

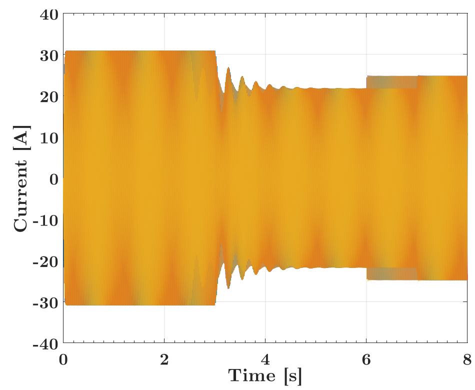

(d) Inverter two currents.

Fig. 5.6: Voltages and currents of both inverters during the planned scenario.

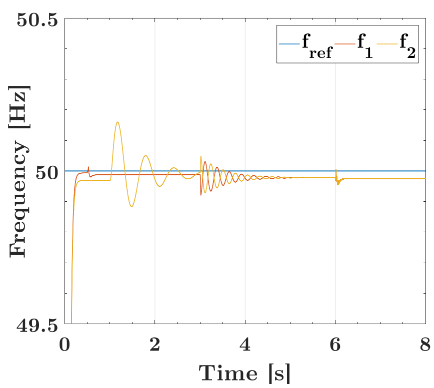

(a) Frequency deviations.

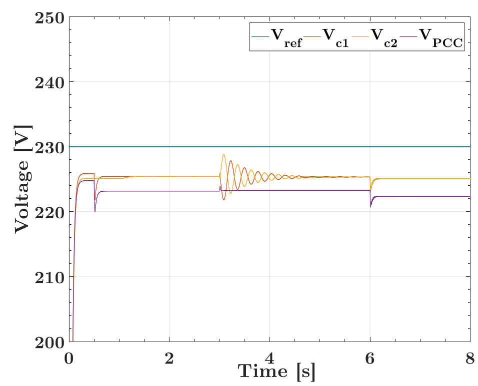

(b) Voltage deviations.

Fig. 5.7: Deviations of frequency and voltage due to the droop control and the load changes.

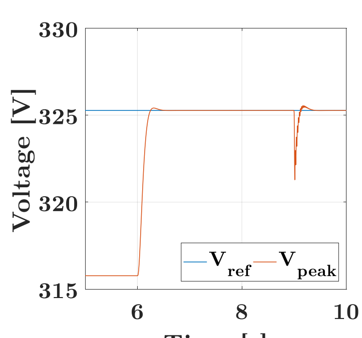

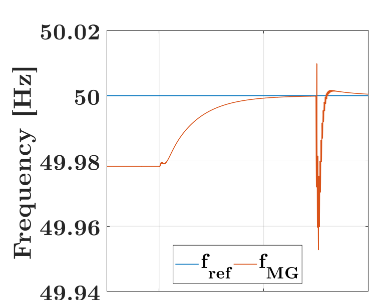

Once the centralized secondary control has been validated, also the decentralized one has been tested. Also in this case the secondary begun its action at six seconds and a step change in the load occurs at nine seconds. The voltage and frequency response can be seen in the following figure.

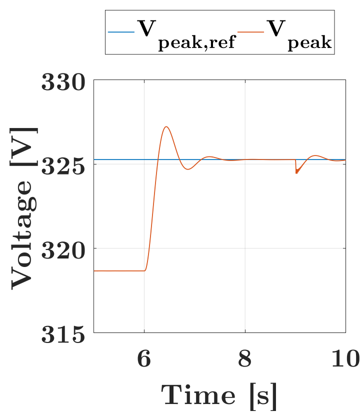

(a) Voltage deviation of the d component of the capacitor voltage.

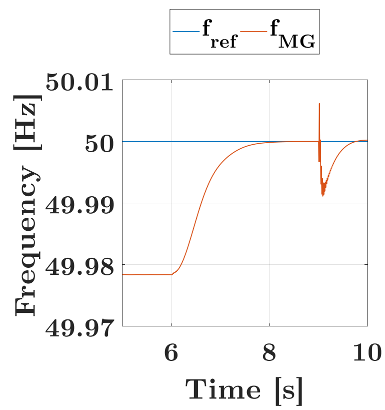

(b) Comparison between the reference frequency and the Microgrid measured one.

Fig. 5.9: Deviations of frequency and amplitude of the Microgrid voltage when the decentralized secondary control is employed.

5.2 Grid-connected Mode

So far, only the operation of the MG in islanded mode has been analyzed. Since the synchronization procedure while connecting to the main grid is a critical transition, in this section its details are verified.

As first, the deviations of frequency and amplitude between the Microgrid and the main grid are shown in Fig.5.10. In this project, the main has been considered stiff (i.e. no frequency and no voltage variations).

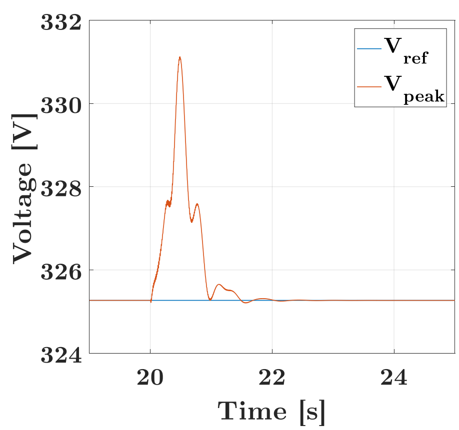

(a) Behavior of voltage during connection to the grid.

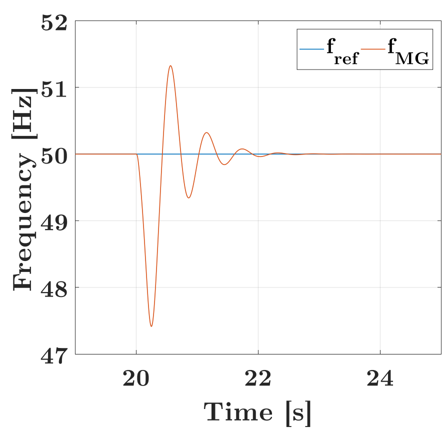

(b) Behavior of frequency during connection to the grid.

Fig. 5.10: Transient of voltage and frequency during the grid connection.

As can be seen, even if there is a peak in the d-component of the Microgrid voltage when the main grid is connected, the system goes to steady-state in around three seconds. Regarding the frequency response, even though it present some oscillations, it reaches the reference value in three seconds as well.

Another important aspect to be verified is the ability of the system to track the reference powers. Hereafter the case when the Microgrid is absorbing power from the maing grid is considered.

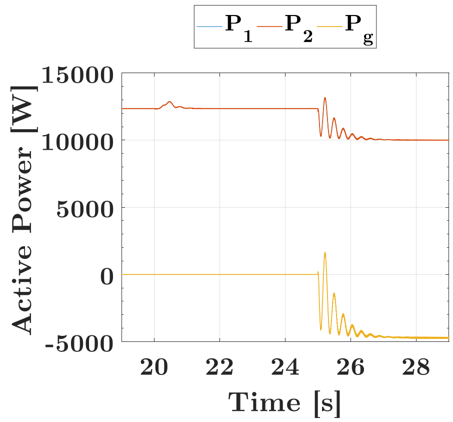

(a) Active power of the converters in the MG and of the grid.

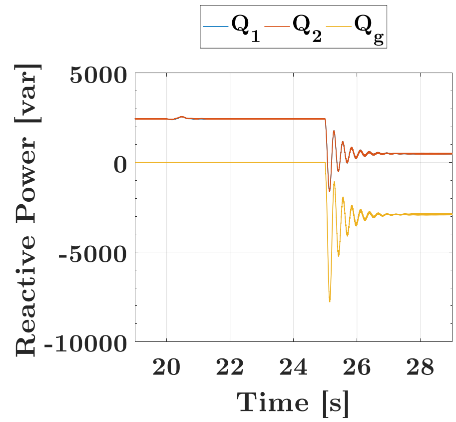

(b) Reactive power of the converters in the MG and of the grid.

Fig. 5.11: Active and reactive power of both the converters inside the Microgrid and the main grid.

As can be seen, the grid is providing active power since the MG load is higher than its energy production. Furthermore, the main grid is also supplying more reactive power than the one needed by the loads. This can be due to the reactive power dissipated by the reactive components in the MG.

Finally, the currents of both VSIs and of the main grid are shown in Fig.5.12. The figure shows that even though there are some oscillations when the Microgrid is connected to the grid, the aren't particularly high overshoots so that any further control action is needed.

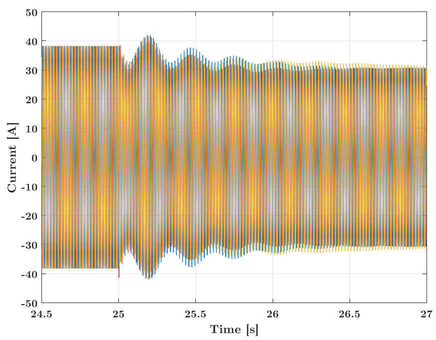

(a)

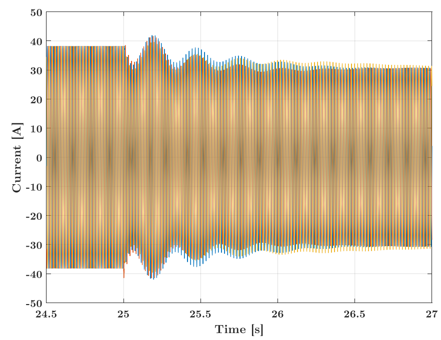

(b)

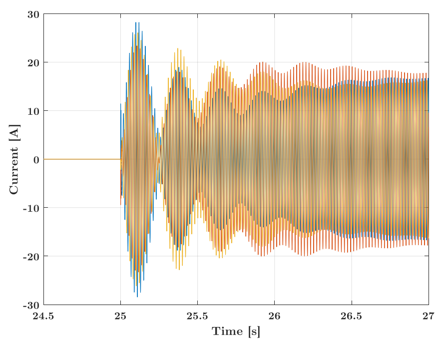

(c)

Fig. 5.12: Three phase currents of a) inverter one, b) inverter two and c) of the grid.

Chapter 6

Conclusions and future work

6.1 Summary

The focus of this thesis work has been on the hierarchical control of an AC Microgrid. In the first section, the status of the nowadays main grid and the effects of the penetration of DERs have been analyzed. After this, the benefits of the employment of MGs have been listed. Further, a brief overview of the general structure of a Microgrid and its control possibilities have been carried out. Among them, the AC Microgrid controlled with a hierachical control seems to be the best solution. The topics treated in the second section of the thesis are related to the design of the parameters of the first two levels of the hierarchy. Along with the design, the theoretical aspects of the control loops have been analyzed.

To validate the designed control, a simulation model has been built. The analysis started from the islanded mode, where all the control have been tested. First, the primary control has been tested with only one inverter. The working principles of droop, current and voltage loops have been validated. Then, a second inverter has been introduced with the aim to validate the synchronization loop. Despite from the presented results, the voltage and frequency variations are within the limits, two types of secondary control have been implemented: the centralized and the distributed. Indeed the Microgrid has to fulfil the grid standards to be able to supply the loads correctly, eliminating the the deviations from the nominal values of the frequency and of the voltage. What emerged is that the distributed secondary control presents lower peaks in the frequency and voltage deviations during the transients. During all the tests, a discrepancy in the reactive power measurement has been experienced but, with the introduction of the distributed secondary this discrepancy is lower thanks to the reactive power flow control.

Lastly, the Microgrid has been connected to a stiff grid. From the presented results, even though there are some peaks in the voltage and in the frequency when the switch closes, it results clear that the developed control is able to ensure the proper connection of the MG with the main grid. Furthermore, from the power flow point of view, the droop control is able to track the active and reactive power references. Anyway, the grid is supplying more reactive power than requested. This can be addressed to the power losses in the grid-side filter and to the line impedance.

6.2 Future Work

The work done in this thesis can be improved under several points of view. First, considering the primary level, a PR-based current control can be used in order to improve the time response of the system, especially in presence of non linear loads. Moreover, this simplifies the implementation of the harmonic compensation. Another important aspect that should be added is the stability analysis, in order to understand the influence of the line parameters on the system stability. Since the line impedance components may vary, a virtual impedance may be implemented to ensure that the output impedance of the inverter is constant.

Regarding the secondary control, two aspects can be introduced. One is the analysis of the impact of the communication delay in the centralized secondary. Another is the implementation of an optimization algorithm for the energy management when the MG is in islanded mode.

Since in this thesis the tertiary has not been implemented, the hierarchical control analysis can be completed with its introduction. The benefit related to this addition is the management of the power flow towards the grid, perhaps considering optimization aspects such as energy price, grid congestion and clustering of several MGs.

Concluding, such control implementation shall be tested throughout experimental results in both islanded and grid-connected mode. Additionally, the Internet of Things (IoT) interaction may be of a research interest for energy management improvement.

Appendices

Appendix A

Power Calculation

Taking into consideration the system in Fig.A.1, that is reported hereafter for sake of simplicity, the equations of the active and reactive power can be derived.

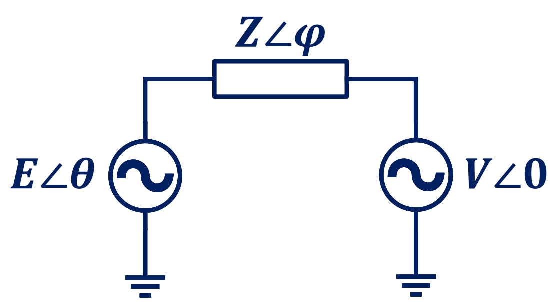

Fig. A.1: Connection of a DG inverter to the grid through a complex feeder.

First, the current I can be written in its vector form as:

$$\bar{\mathbf{I}} = \frac{\overline{\mathbf{E}} - \overline{\mathbf{V}}}{\overline{Z}} \tag{A.1}$$

Expressing the quantities in the right part of the Eq.A.1 in the complex form, the following equation can be written:

$$\bar{\mathbf{I}} = \frac{cos\varphi - jsin\varphi}{Z} \cdot (Ecos\theta - V + jEsin\theta) =$$
$$\frac{Ecos\theta cos\varphi - Vcos\varphi + jEsin\theta cos\varphi - jEcos\theta sin\varphi + jVsin\varphi + Esin\theta sin\varphi}{Z}$$

From here, the complex conjugate of the current $\overline{\mathbf{I*}}$ can be calculated and finally the complex power can be written as:

$$\overline{\mathbf{S}} = \overline{\mathbf{V}} \cdot \overline{\mathbf{I*}} \tag{A.2}$$

Finally the equations for the active and reactive power are shown in Eq.A.3 and Eq.A.4.

$$P = \Re\left\{\overline{\mathbf{S}}\right\} = \left(\frac{VEcos\theta}{Z} - \frac{V^2}{Z}\right)cos\varphi + \frac{VEsin\theta}{Z}sin\varphi \tag{A.3}$$

$$Q = \Im\left\{\overline{\mathbf{S}}\right\} = \left(\frac{VEcos\theta}{Z} - \frac{V^2}{Z}\right)sin\varphi - \frac{VEsin\theta}{Z}cos\varphi \tag{A.4}$$

Bibliography

[1] OECD Publishing. *World Energy Balances 2017*. OECD Publishing, Paris, 2017.

[2] Bert Brunekreef and Stephen T Holgate. Air pollution and health. *The lancet*, 360(9341):1233–1242, 2002.

[3] Stephen T Holgate, Hillel S Koren, Jonathan M Samet, and Robert L Maynard. *Air pollution and health*. Elsevier, 1999.

[4] Robert Lasseter, Abbas Akhil, Chris Marnay, John Stephens, Jeff Dagle, Ross Guttromson, A Sakis Meliopoulous, Robert Yinger, and Joe Eto. Integration of distributed energy resources. the certs microgrid concept. *white paper*, 2002.

[5] Jonathan Liao Mattin Grao Txapartegi, Dr Ana Villamor. Status of the power electronics industry 2017. Technical report, Yole Développment, 07 2017.

[6] Juan C Vasquez, Josep M Guerrero, Mehdi Savaghebi, Joaquin Eloy-Garcia, and Remus Teodorescu. Modeling, analysis, and design of stationary-reference-frame droop-controlled parallel three-phase voltage source inverters. *IEEE Transactions on Industrial Electronics*, 60(4):1271–1280, 2013.

[7] Phil Barker and Doug Herman. Technical and economic feasibility of microgrid-based power systems. In *Seventh EPRI Distributed Resources Conference and Exhibition Dallas*, pages 20–22, 2002.

[8] Jackson John Justo, Francis Mwasilu, Ju Lee, and Jin-Woo Jung. Ac-microgrids versus dc-microgrids with distributed energy resources: A review. *Renewable and Sustainable Energy Reviews*, 24:387–405, 2013.

[9] Magdi S Mahmoud, S Azher Hussain, and MA Abido. Modeling and control of microgrid: An overview. *Journal of the Franklin Institute*, 351(5):2822–2859, 2014.

[10] Peter M Curtis. *Maintaining mission critical systems in a 24/7 environment*, volume 61. John Wiley & Sons, 2011.

[11] Josep M Guerrero and Frede Blaabjerg. Smart grid and renewable energy systems. *IEEE International Conference on Electrical Machines and Systems (ICEMS)*, 2011.

[12] Robert H Lasseter. Microgrids. In *Power Engineering Society Winter Meeting, 2002. IEEE*, volume 1, pages 305–308. IEEE, 2002.

[13] Magdi S Mahmoud. *Microgrid: Advanced Control Methods and Renewable Energy System Integration*. Elsevier, 2016.

[14] Fanghong Guo, Changyun Wen, and Yong-Duan Song. *Distributed Control and Optimization Technologies in Smart Grid Systems*. CRC Press, 2017.

[15] Eneko Unamuno and Jon Andoni Barrena. Hybrid ac/dc microgrids—part i: Review and classification of topologies. *Renewable and Sustainable Energy Reviews*, 52:1251–1259, 2015.

[16] Office of Electricity Delivery and Sandia National Laboratories Energy Reliability. Doe global energy storage database, April 2018.

[17] Mohamed A Awadallah and Bala Venkatesh. Energy storage in flywheels: An overview. *Canadian Journal of Electrical and Computer Engineering*, 38(2):183–193, 2015.

[18] Vladimir S Bagotsky, Alexander M Skundin, and Yurij M Volfkovich. *Electrochemical power sources: batteries, fuel cells, and supercapacitors*. John Wiley & Sons, 2015.

[19] Catia Arbizzani, M Mastragostino, and F Soavi. New trends in electrochemical supercapacitors. *Journal of power sources*, 100(1-2):164–170, 2001.

[20] S Ould Amrouche, Djamila Rekioua, Toufik Rekioua, and Seddik Bacha. Overview of energy storage in renewable energy systems. *International Journal of Hydrogen Energy*, 41(45):20914–20927, 2016.

[21] Electrical Energy Storage. Iec white paper, 2011.

[22] MIRUS International Inc. Harmonic mitigating transformers/faq's,what are nonlinear loads and why are they a concern today?, 2003.

[23] Mircea Eremia and Mohammad Shahidehpour. *Handbook of electrical power system dynamics: modeling, stability, and control*, volume 92. John Wiley & Sons, 2013.

[24] Leslie Hewitson, Mark Brown, and Ramesh Balakrishnan. *Practical power system protection*. Elsevier, 2004.

[25] Ali Keyhani and Muhammad Marwali. *Smart power grids 2011*. Springer, 2012.

[26] Hannu Jaakko Laaksonen. Protection principles for future microgrids. *IEEE Transactions on Power Electronics*, 25(12):2910–2918, 2010.

[27] Frede Blaabjerg, Yongheng Yang, Dongsheng Yang, and Xiongfei Wang. Distributed power-generation systems and protection. *Proceedings of the IEEE*, 105(7):1311–1331, 2017.

[28] Mohammad Hadi Andishgar, Eskandar Gholipour, and Rahmat-allah Hooshmand. An overview of control approaches of inverter-based microgrids in islanding mode of operation. *Renewable and Sustainable Energy Reviews*, 80:1043–1060, 2017.

[29] ChengShan Wang, XiaLin Li, Li Guo, and YunWei Li. A seamless operation mode transition control strategy for a microgrid based on master-slave control. *Science China Technological Sciences*, 55(6):1644–1654, 2012.

[30] Jiann-Fuh Chen and Ching-Lung Chu. Combination voltage-controlled and current-controlled pwm inverters for ups parallel operation. *IEEE Transactions on Power Electronics*, 10(5):547–558, 1995.

[31] Xiao Sun, Yim-Shu Lee, and Dehong Xu. Modeling, analysis, and implementation of parallel multi-inverter systems with instantaneous average-current-sharing scheme. *IEEE Transactions on Power Electronics*, 18(3):844–856, 2003.

[32] Tsai-Fu Wu, Yu-Kai Chen, and Yong-Heh Huang. 3c strategy for inverters in parallel operation achieving an equal current distribution. *IEEE Transactions on Industrial Electronics*, 47(2):273–281, 2000.

[33] Daniel E Olivares, Ali Mehrizi-Sani, Amir H Etemadi, Claudio A Cañizares, Reza Iravani, Mehrdad Kazerani, Amir H Hajimiragha, Oriol Gomis-Bellmunt, Maryam Saeedifard, Rodrigo Palma-Behnke, et al. Trends in microgrid control. *IEEE Transactions on smart grid*, 5(4):1905–1919, 2014.

[34] Takao Kawabata and Shigenori Higashino. Parallel operation of voltage source inverters. *IEEE Transactions on Industry Applications*, 24(2):281–287, 1988.

[35] Josep M Guerrero, Juan C Vasquez, José Matas, Luis García De Vicuña, and Miguel Castilla. Hierarchical control of droop-controlled ac and dc microgrids—a general approach toward standardization. *IEEE Transactions on industrial electronics*, 58(1):158–172, 2011.

[36] Josep M Guerrero, Mukul Chandorkar, Tzung-Lin Lee, and Poh Chiang Loh. Advanced control architectures for intelligent microgrids—part i: Decentralized and hierarchical control. *IEEE Transactions on Industrial Electronics*, 60(4):1254–1262, 2013.

[37] Ali Bidram and Ali Davoudi. Hierarchical structure of microgrids control system. *IEEE Transactions on Smart Grid*, 3(4):1963–1976, 2012.

[38] Juan C Vasquez, Josep M Guerrero, Jaume Miret, Miguel Castilla, and Luis Garcia De Vicuna. Hierarchical control of intelligent microgrids. *IEEE Industrial Electronics Magazine*, 4(4):23–29, 2010.

[39] Allal M Bouzid, Josep M Guerrero, Ahmed Cheriti, Mohamed Bouhamida, Pierre Sicard, and Mustapha Benghanem. A survey on control of electric power distributed generation systems for microgrid applications. *Renewable and Sustainable Energy Reviews*, 44:751–766, 2015.

[40] DG Holmes, TA Lipo, BP McGrath, and WY Kong. Optimized design of stationary frame three phase ac current regulators. *IEEE Transactions on Power Electronics*, 24(11):2417–2426, 2009.

[41] Daniel Nahum Zmood and Donald Grahame Holmes. Stationary frame current regulation of pwm inverters with zero steady-state error. *IEEE Transactions on power electronics*, 18(3):814–822, 2003.

[42] Frede Blaabjerg, Remus Teodorescu, Marco Liserre, and Adrian V Timbus. Overview of control and grid synchronization for distributed power generation systems. *IEEE Transactions on industrial electronics*, 53(5):1398–1409, 2006.

[43] Charles L Phillips and John M Parr. *Feedback control systems*. Pearson, 2011.

[44] Daniel Nahum Zmood, Donald Grahame Holmes, and Gerwich H Bode. Frequency-domain analysis of three-phase linear current regulators. *IEEE Transactions on Industry Applications*, 37(2):601–610, 2001.

[45] Klaas Visscher and Sjoerd Walter Hero De Haan. Virtual synchronous machines (vsg's) for frequency stabilisation in future grids with a significant share of decentralized generation. In *SmartGrids for Distribution, 2008. IET-CIRED. CIRED Seminar*, pages 1–4. IET, 2008.

[46] MC Chandrokar, DM Divan, and B Banerjee. Control of distributed ups systems. 1:197–204, 1994.

[47] Alexander Micallef, Maurice Apap, Cyril Spiteri-Staines, and Josep M Guerrero. Single-phase microgrid with seamless transition capabilities between modes of operation. *IEEE Transactions on Smart Grid*, 6(6):2736–2745, 2015.

[48] Directorate-General for Energy European Commission. Commission regulation (eu) 2017/1485 of 2 august 2017 establishing a guideline on electricity transmission system operation, aug 2017.

[49] Guan Yajuan, Wu Weiyang, Guo Xiaoqiang, and Gu Herong. An improved droop controller for grid-connected voltage source inverter in microgrid. In *Power Electronics for Distributed Generation Systems (PEDG), 2010 2nd IEEE International Symposium on*, pages 823–828. IEEE, 2010.

[50] Estefanía Planas, Asier Gil-de Muro, Jon Andreu, Iñigo Kortabarria, and Iñigo Martínez de Alegría. General aspects, hierarchical controls and droop methods in microgrids: A review. *Renewable and Sustainable Energy Reviews*, 17:147–159, 2013.

[51] Usman Bashir Tayab, Mohd Azrik Bin Roslan, Leong Jenn Hwai, and Muhammad Kashif. A review of droop control techniques for microgrid. *Renewable and Sustainable Energy Reviews*, 76:717–727, 2017.

[52] Ramin Moslemi and Javad Mohammadpour. Accurate reactive power control of autonomous microgrids using an adaptive virtual inductance loop. *Electric Power Systems Research*, 129:142–149, 2015.

[53] X. Wang, X. Yue D. Yang, and D. Pan D.Lu. Slide deck of the course: Design-oriented grid converter dynamics in renewable and traction systems, 2017.

[54] Hassan Bevrani. *Robust power system frequency control*. Springer, 2014.

[55] Thangaiah Jesintha Mary and Parthasarathy Rangarajan. Delay-dependent stability analysis of microgrid with constant and time-varying communication delays. *Electric Power Components and Systems*, 44(13):1441–1452, 2016.

[56] Qobad Shafiee, Josep M Guerrero, and Juan C Vasquez. Distributed secondary control for islanded microgrids—a novel approach. *IEEE Transactions on power electronics*, 29(2):1018–1031, 2014.

[57] A Reznik, M Godoy Simoes, Ahmed Al-Durra, and SM Muyeen. Lcl filter design and performance analysis for small wind turbine systems. In *Power Electronics and Machines in Wind Applications (PEMWA), 2012 IEEE*, pages 1–7. IEEE, 2012.